The Abdus Salam International Centre for Theoretical Physics

United Nations Educational, Scientific and Cultural Organization

IAEA International Atomic Energy Agency

1953-25

International Workshop on the Frontiers of Modern Plasma Physics

14 - 25 July 2008

Landau fluid models for collisionless plasmas.

P.L. Sulem

Observatoire de la Cote D'Azur
Nice
France

Landau fluid models for collisionless plasmas

Pierre-Louis Sulem and Thierry Passot
CNRS, Observatoire de la Côte d'Azur, Nice

The Frontiers of Modern Plasma Physics
ICTP, Trieste, 14-18 July 2008

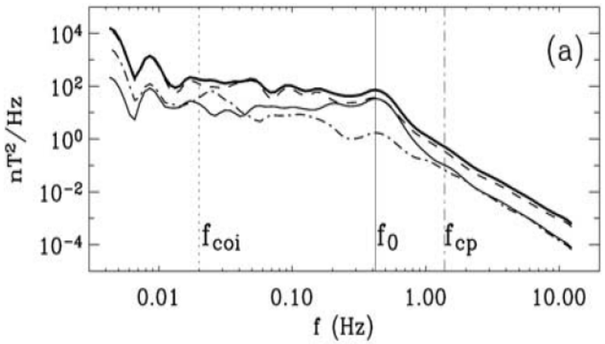

Magnetic energy spectrum in the magnetosheath downstream of the bow shock (Alexandrova et al., JGR, 2006).

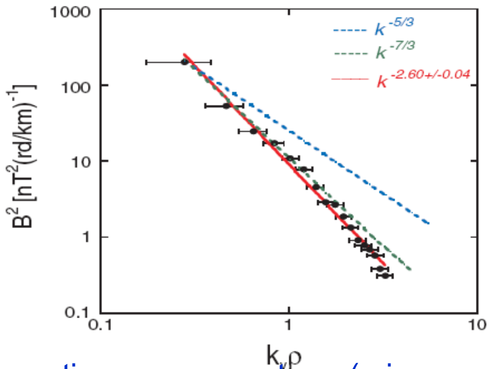

Magnetic energy spectrum (mirror modes) in the magnetosheath close to the magnetopause (Sahraoui et al., PRL 2006)

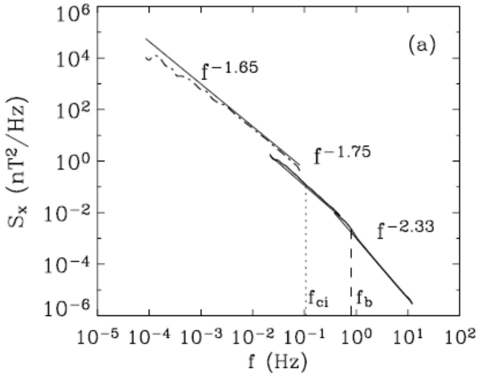

Solar wind turbulent spectrum (Alexandrova et al., 2007)

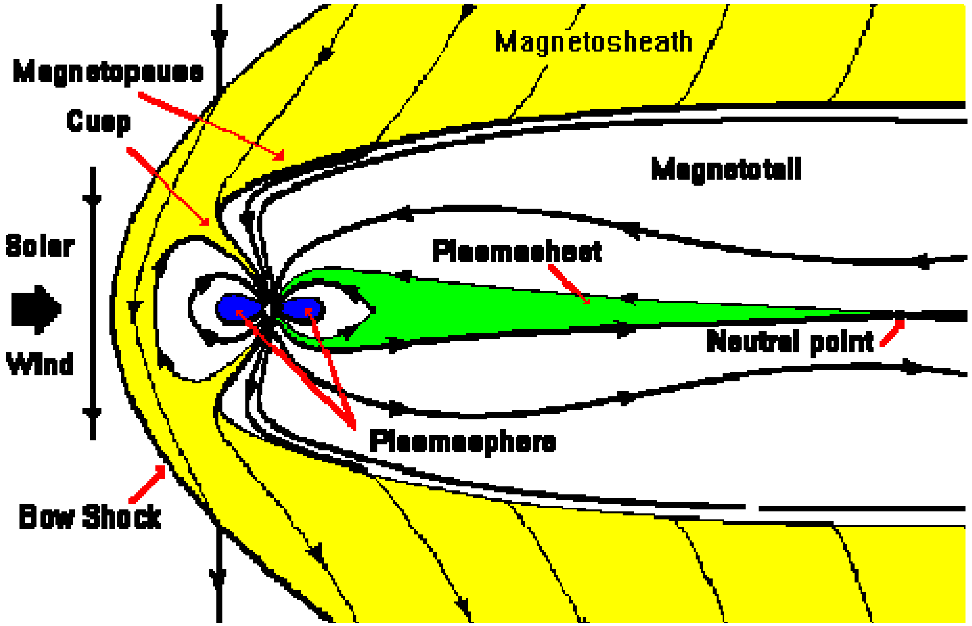

Space plasmas such as the solar wind or the magnetosheath are turbulent magnetized plasmas with essentially no collisions.

High quality in situ measurements (CLUSTER, etc.)

Observed cascades extend beyond the ion Larmor radius: kinetic effects play a significant role.

Another issue:

Formation and evolution of small-scale coherent structures
(filaments, shocklets, magnetosonic solitons, magnetic holes)
observed in various spatial environments.

Typical length scale of the structures: a few ion Larmor radii.

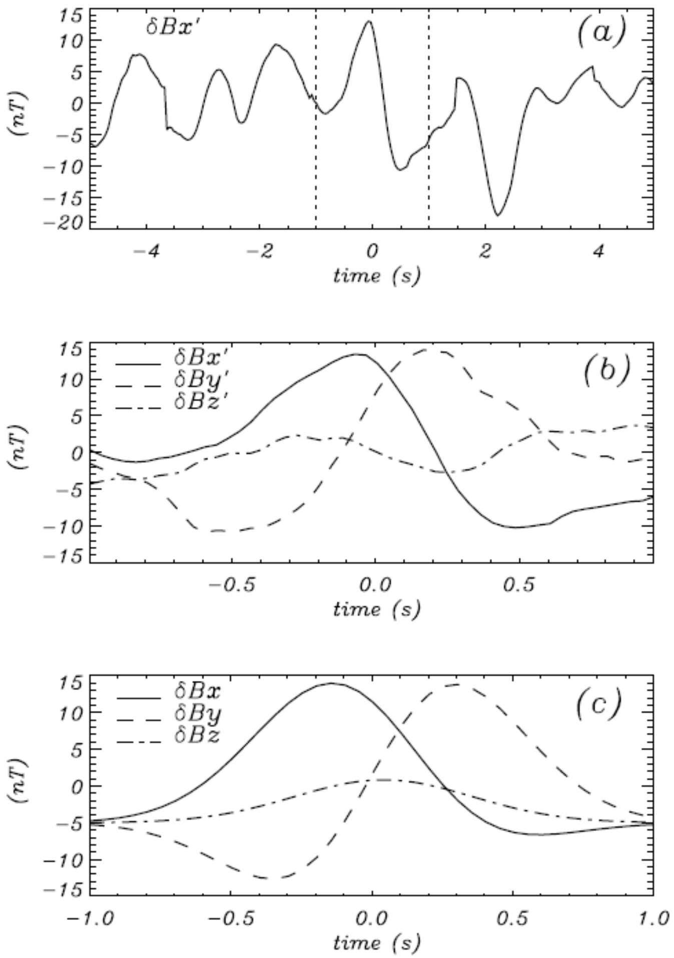

Figure 8. Magnetic field fluctuations, taking $\tau \simeq -420$ s (1755:16 UT) as the origin of time. (a) Fluctuations $\delta B_{x'}$ during 10 s around τ. (b) Fluctuations of the magnetic field components ($\delta B_{x'}$, $\delta B_{y'}$, $\delta B_{z'}$) for the 2-s period around τ. (c) The z-aligned current tube simulation (δB_x, δB_y, δB_z).

Signature of magnetic filaments
(Alexandrova et al. JGR 2004)

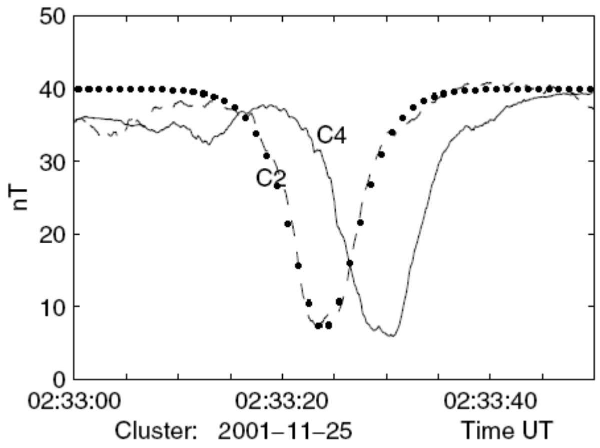

FIG. 1. A large scale soliton observed by Cluster spacecraft C2 (dashed) and C4 (solid) in the total magnetic field. Marked curve shows fit of $b_0 \operatorname{sech}^2[(t - t_0)/\delta t]$ with $b_0 = -33$ nT and $\delta t = 4.4$ s. The soliton moves with velocity $u_0 \approx 250$ km/s and has a width of 2000 km. The position of Cluster satellites was $(-4, 17, 5)$ R_E GSE.

Slow magnetosonic solitons
(Stasiewicz et al. PRL 2003)

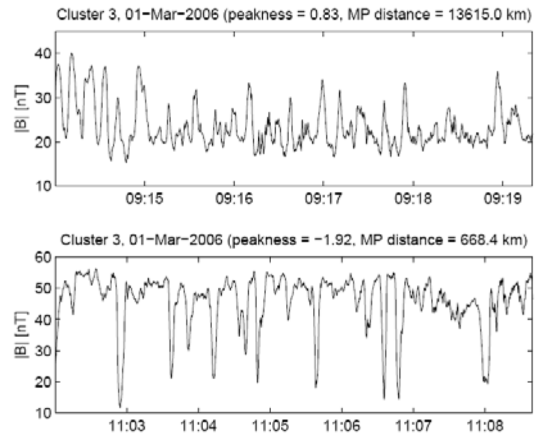

Mirror structures in the terrestrial magnetosheath
(Soucek et al.JGR 2008)

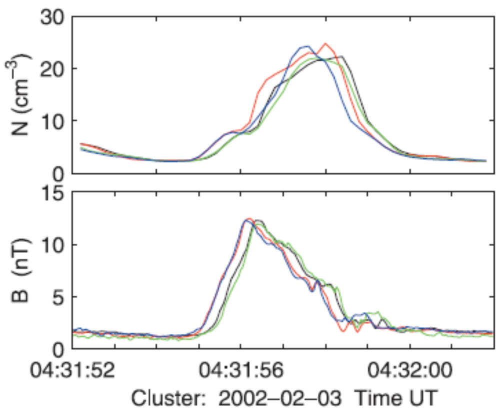

Figure 2. Pulse-like enhancements of the plasma density and magnetic field measured on four Cluster spacecraft: C1–C4, which are color coded in sequence: black, red, green, blue. The measurements represent signatures of fast magnetosonic shocklets moving with supersonic speed in a high-β plasma.

fast magnetosonic shocklets
(Stasiewicz et al. GRL 2003)

Strictly speaking, collisionless plasmas require a kinetic description,

because of

- the closure problem for the hierarchy of equations governing the fluid moments

- wave-particle resonances such as the Landau damping

- the possible finite Larmor radius effects

Computational cost of kinetic simulations in turbulent regimes is very high,even in the gyrokinetic description that

involves averaging on the particle gyromotion

is restricited to quasi-transverse low-frequency dynamics

Question: Can fluid models provide an "approximate" alternative to kinetic descriptions of low-frequency phenomena in magnetized collisionless plasmas?

Two main approaches:

Closing the hierarchy derived from Vlasov-Maxwell equations: Landau fluids

Closing the hierarchy derived from gyrokinetic equation: gyrofluids

Landau fluids:

- Introduced by Hammett & Perkins (1990) as approximate closures retaining phase mixing and linear Landau damping.

- Implemented in the context of large-scale MHD by Snyder, Hammett & Dorland (1997) to close the hierarchy of moment equations derived from the drift kinetic equation: retain *Landau damping*.

- Extended to dispersive MHD by including *large-scale FLR corrections* computed perturbatively within the fluid formalism (derived from Vlasov-Maxwell equations) [Goswami, Passot & Sulem, PoP 2005].

- Further extension aimed to resolve transverse scales comparable to or smaller than the ion gyroradius: "FLR-Landau fluid" [Passot & Sulem, PoP 14, 082502, 2007].

FLR-Landau-fluids include a full description of the hydrodynamic nonlinearities, supplemented by a **linear** (or semi-linear when the instantaneous variations of the plasma mean quantities, such as pressures, are retained) description of low-frequency kinetic effects.

Alternative approach: gyrofluids

(Brizard 1992, Dorland & Hammett 1993, Beer & Hammett 1996, Scott 2005)

- Obtained by taking velocity moments of the gyrokinetic equation.

- Nonlinear FLR corrections to all orders are captured.

- Involve a linear closure of the hierarchy, as the Landau fluids.

- Equations are rather complex because not written in the physical coordinates but in the gyrocenter variables. The transformation from one set of variables to the other requires additional approximations.

- All fast magnetosonic waves [that may contribute to the turbulent cascade (Luo & Melrose 07)] are ordered out, while FLR-Landau fluids retain large-scale fast magnetosonic waves.

Both Landau fluids and gyrofluid neglect wave particle trapping, i.e. the effect of particle bounce motion on the distribution function near resonance.

Landau fluids

For the sake of simplicity, neglect electron inertia.

Ion dynamics: derived by computing velocity moments from Vlasov Maxwell equations.

$$\partial_t \rho_p + \nabla \cdot (\rho_p u_p) = 0$$

$$\partial_t u_p + u_p \cdot \nabla u_p + \frac{1}{\rho_p} \nabla \cdot \mathbf{p}_p - \frac{e}{m_p}(E + \frac{1}{c} u_p \times B) = 0$$

$$E = -\frac{1}{c}\Big(u_p - \frac{j}{ne}\Big) \times B - \frac{1}{ne} \nabla \cdot \mathbf{p}_e,$$

$$\partial_t B = -c \nabla \times E$$

$$\rho_r = m_r n_r$$

quasi-neutrality $(n_e = n_p)$

$$j = \frac{c}{4\pi} \nabla \times B$$

$\mathbf{p}_p = p_{\perp p} \mathbf{n} + p_{\| p} \boldsymbol{\tau} + \mathbf{\Pi}$, with $\mathbf{n} = \mathbf{I} - \widehat{b} \otimes \widehat{b}$ and $\boldsymbol{\tau} = \widehat{b} \otimes \widehat{b}$, where $\widehat{b} = B / |B|$.

Electron pressure tensor is taken gyrotropic (scales >> electron Larmor radius): characterized by the parallel and transverse pressures $p_{\| e}$ and $p_{\perp e}$.

For each particle species,

Perpendicular and parallel pressures

heat flux tensor

$$\partial_t p_\perp + \nabla \cdot (u p_\perp) + p_\perp \nabla \cdot u - p_\perp \hat{b} \cdot \nabla u \cdot \hat{b} + \frac{1}{2}[\mathrm{tr}\ \nabla \cdot \mathbf{q} - \hat{b} \cdot (\nabla \cdot \mathbf{q}) \cdot \hat{b}] = 0$$

$$\partial_t p_\parallel + \nabla \cdot (u p_\parallel) + 2 p_\parallel \hat{b} \cdot \nabla u \cdot \hat{b} + \hat{b} \cdot (\nabla \cdot \mathbf{q}) \cdot \hat{b} = 0$$

Nongyrotropic components of the pressure tensor *(gyroviscous tensor)* will be evaluated separately by fitting with the linear kinetic theory.

Heat fluxes

$\mathbf{n} = \mathbf{I} - \widehat{b} \otimes \widehat{b}$ and $\boldsymbol{\tau} = \widehat{b} \otimes \widehat{b}$, where $\widehat{b} = B / |B|$

Proton heat flux tensor: $\mathbf{q} = \mathbf{S} + \boldsymbol{\sigma}$ with $\sigma_{ijk} n_{jk} = 0$ and $\sigma_{ijk} \tau_{jk} = 0$.

Nongyrotropic tensor that contributes
at the nonlinear level only

Fluxes of parallel and transverse heat: $S_i^{\|} = q_{ijk}\tau_{jk}$ and $2S_i^{\perp} = q_{ijk} n_{jk}$.

Parallel heat fluxes of perpendicular and parallel heat $q_\perp = S^\perp \cdot \widehat{b}$ and $q_\| = S^\| \cdot \widehat{b}$ are the only contribution to the gyrotropic heat flux tensor.

Write $S^\perp = q_\perp \widehat{b} + S_\perp^\perp$ and $S^\| = q_\| \widehat{b} + S_\perp^\|$ where the perpendicular heat flux of perpendicular and parallel heat $S_\perp^\perp$ and $S_\perp^\|$ are computed in a linearized approximation.

The gyrotropic heat flux components $q_\perp$ and $q_\|$ obey dynamical equations.

Equations for the parallel and perpendicular (gyrotropic) heat fluxes

$$\begin{cases} \partial_t q_\| + \nabla\cdot(q_\| u) + 3q_\|\widehat{b}\cdot\nabla u\cdot\widehat{b} + 3p_\|(\widehat{b}\cdot\nabla)\left(\frac{p_\|}{\rho}\right) + \nabla\cdot(\widetilde{r}_{\|\|}\widehat{b}) - 3\widetilde{r}_{\|\perp}\nabla\cdot\widehat{b} + \partial_z R_\|^{NG} = 0 \\ \partial_t q_\perp + \nabla\cdot(u q_\perp) + q_\perp\nabla\cdot u + p_\|(\widehat{b}\cdot\nabla)\left(\frac{p_\perp}{\rho}\right) + \frac{p_\perp}{\rho}\left(\partial_x\Pi_{xz} + \partial_y\Pi_{yz}\right) \\ \qquad + \nabla\cdot(\widetilde{r}_{\|\perp}\widehat{b}) + \left((p_\| - p_\perp)\frac{p_\perp}{\rho} - \widetilde{r}_{\perp\perp} + \widetilde{r}_{\|\perp}\right)(\nabla\cdot\widehat{b}) + \partial_z R_\perp^{NG} = 0 \end{cases}$$

Involve the 4 th rank gyrotropic cumulants $\widetilde{r}_{\|\|}, \widetilde{r}_{\|\perp}, \widetilde{r}_{\perp\perp}$
expressed in terms of the 4 th rank gyrotropic moments by

$$\widetilde{r}_{\|\|} = r_{\|\|} - 3\frac{p_\|^2}{\rho},$$

$$\widetilde{r}_{\|\perp} = r_{\|\perp} - \frac{p_\perp p_\|}{\rho},$$

$$\widetilde{r}_{\perp\perp} = r_{\perp\perp} - 2\frac{p_\perp^2}{\rho}.$$

$R_\|^{NG}$ and $R_\perp^{NG}$ stand for the nongyrotropic contributions of the fourth rank cumulants.

2 main problems:

(1) Closure relations are needed to express the 4th order cumulants $\widetilde{r}_{\parallel\parallel}$, $\widetilde{r}_{\parallel\perp}$, $\widetilde{r}_{\perp\perp}$
(closure at lowest order also possible, although usually less accurate)

(2) (Non-gyrotropic) FLR corrections to the various moments are to be evaluated

The starting point for addressing these points is the linear kinetic theory in the low-frequency limit. $\omega/\Omega \sim \epsilon \ll 1$ (Ω: ion gyrofrequency)

For a unified description of fluid and kinetic scales, FLR-Landau fluids retain contributions of:

- quasi-transverse fluctuations $(k_\parallel/k_\perp \sim \epsilon)$ with $k_\perp r_L \sim 1$
- hydrodynamic scales with $k_\parallel r_L \sim k_\perp r_L \sim \epsilon.$

r_L : ion Larmor radius

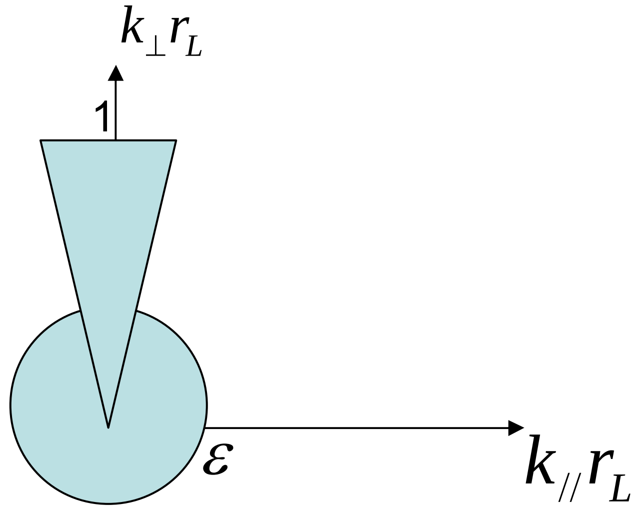

CLOSURE RELATIONS are based on linear kinetic theory (near bi-Maxwellian equilibrium) in the low-frequency limit.

For example, for each species, (assuming the ambient magnetic field along the z direction),

$$\widetilde{r}_{\parallel\perp} = \frac{{p_\perp^{(0)}}^2}{\rho^{(0)}}\left[1 - R(\zeta) + 2\zeta^2 R(\zeta)\right]\left[[2b\Gamma_0(b) - \Gamma_0(b) - 2b\Gamma_1(b)]\frac{b_z}{B_0} + b[\Gamma_0(b) - \Gamma_1(b)]\frac{e\Psi}{T_\perp^{(0)}}\right]$$

$\Gamma_n(b) = e^{-b} I_n(b)$, $b = (k_\perp^2 T_\perp^{(0)})/(\Omega^2 m)$, $I_n(b)$ modified Bessel function, $E_z = -\partial_z \Psi$

R is the plasma response function, $\zeta = \frac{\omega}{|k_\parallel| v_{th}}$. (For electrons, $b \approx 0$, $\Gamma_0 \approx 1$, $\Gamma_1 \approx 0$)

It turns out that $\widetilde{r}_{\parallel\perp}$ can be expressed in terms of perpendicular gyrotropic heat flux $q_\perp$ and of the parallel current j_z. One has

$$\widetilde{r}_{\parallel\perp} = \sqrt{\frac{2T_\parallel^{(0)}}{m}}\frac{1 - R(\zeta) + 2\zeta^2 R(\zeta)}{2\zeta R(\zeta)}\left[q_\perp + [\Gamma_0(b) - \Gamma_1(b)]\frac{p_\perp^{(0)} p_\parallel^{(0)}}{\rho^{(0)} v_A^2}\left(\frac{T_\perp^{(0)}}{T_\parallel^{(0)}} - 1\right)\frac{j_z}{en^{(0)}}\right]$$

The approximation consists in replacing the plasma response function R by the three pole Padé approximant $R_3(\zeta) = \dfrac{2 - i\sqrt{\pi}\zeta}{2 - 3i\sqrt{\pi}\zeta - 4\zeta^2 + 2i\sqrt{\pi}\zeta^3}$.

This leads to the approximation $\dfrac{1 - R(\zeta) + 2\zeta^2 R(\zeta)}{2\zeta R(\zeta)} \approx \dfrac{i\sqrt{\pi}}{-2 + i\sqrt{\pi}\zeta}$.

(A lower order Padé approximant would overestimates the Landau damping in the large ζ limit).

One finally gets a closure relation in the form of the evolution equation (for each species)

$$[\frac{d}{dt} - \frac{2}{\sqrt{\pi}}\sqrt{\frac{2T_\parallel^{(0)}}{m}}\mathcal{H}_z\partial_z]\widetilde{r}_{\parallel\perp} + \frac{2T_\parallel^{(0)}}{m}\partial_z[q_\perp + [\Gamma_0(b) - \Gamma_1(b)]\frac{p_\perp^{(0)}p_\parallel^{(0)}}{\rho^{(0)}v_A^2}(\frac{T_\perp^{(0)}}{T_\parallel^{(0)}} - 1)\frac{j_z}{en^{(0)}}] = 0,$$

In Fourier space, Hilbert transform $\mathcal{H}_z$ reduces to the multiplication by $i\,\mathrm{sgn}\,k_z$.

Improvement: Retain the evolution of the equilibrium state by replacing the (initial) equilibrium pressures and temperatures by the instantaneous fields averaged on space.

In the large-scale limit, $\Gamma_0(0) = 1$ and $\Gamma_1(0) = 0$.

At large scales, FLR effects negligible: pressure and heat flux tensors are gyrotropic.

$\Rightarrow$ "Landau fluid model for collisionless MHD" (Snyder, Hammett, Dorland 1997) .

Can be viewed as an extension of anisotropic MHD, including linear Landau damping (Hilbert transform with respect to the longitudinal coordinate in the closure relations).

Leading order FLR corrections (non gyrotropic contributions to pressure and heat flux tensors) can easily be supplemented. They induce dispersive effects.

I. Validation of the model for scales large compared with the ion gyroradius

Decay and modulational instabilities of circularly polarized Alfvén waves propagating parallel to the ambient field. Comparison with kinetic theory and hybrid simulations.

(Bugnon, Passot & Sulem, NPG. 11 609, 2004).

Decay instability of parallel Alfvén waves in the long-wavelength limit (no dispersion)

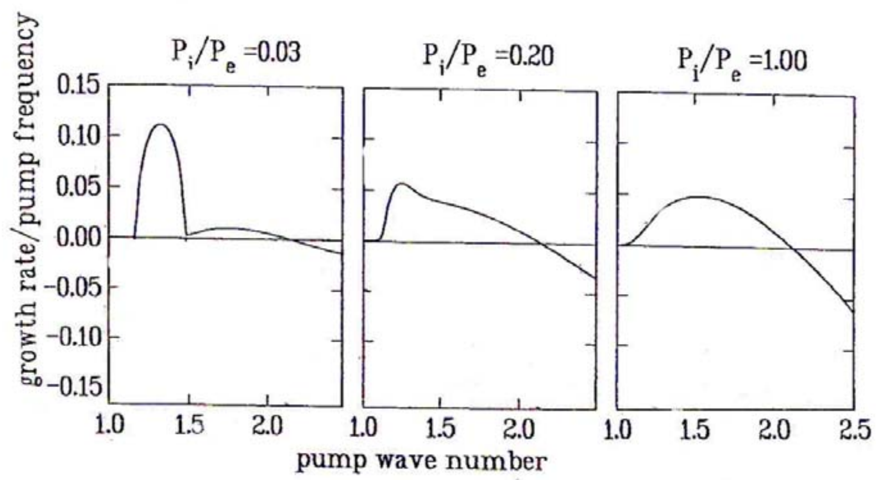

Drift-kinetic analysis (from Inhester 1990)

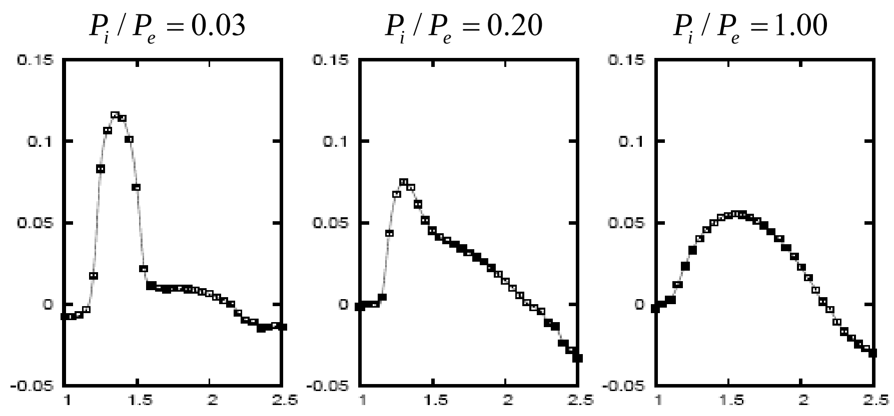

Landau fluid simulation

Maximum growth rates of the density modes versus wavenumber (normalized by the pump wavenumber) resulting from the decay instability of a non dispersive Alfvén wave of amplitude $b_0 = 0.447$ in a plasma with $\beta_{\|p} = 0.3$ and isotropic temperatures such that $T_e^{(0)}/T_p^{(0)} = 33$ (left), $T_e^{(0)}/T_p^{(0)} = 5$ (middle) and $T_e^{(0)}/T_p^{(0)} = 1$ (right).

Reducing electron temperature tends to broaden the spectral range and to reduce the growth rate of the instability.

Decay instability of Alfvén wave produces a forward propagating acoustic wave and a backward Alfvén wave with wavenumber smaller than that of the pump.

Decay instability of a long-wavelength Alfvén pump (continued)

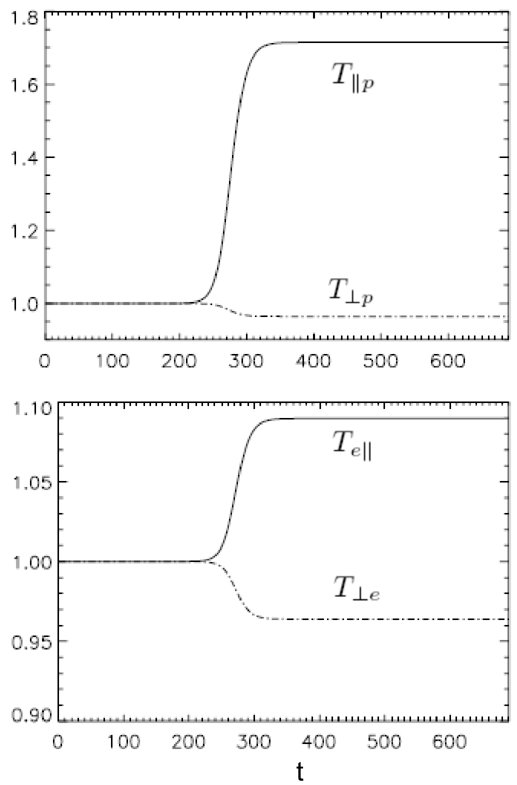

Fig. 3. Time evolution of parallel (solid lines) and transverse (dashed-dotted lines) mean temperatures of the ions (top) and the electrons (bottom) ($P_i / P_e = 1.00$)

Significant parallel heating of the ions
Non negligible parallel heating of the electrons
Cooling in the transverse direction for both ions and electrons.

Decay instability saturates under the effect of Landau damping (rather than mode coupling)

Decay instability of **dispersive** Alfvén waves (continued)

$T_p^{(0)}=T_e^{(0)}$, $\beta_{\parallel p}=0.21$ (corresponding to $\beta=0.42$), and a forward-propagating, right-hand polarized pump with amplitude $u_0=0.1$ and wave number $k_0=4\times 2\pi/D=0.64$ when $D=6.25\times 2\pi$ (in units of ion inertial length).

Decay instability makes the density mode m=6 to be the most unstable at short time. Saturation by Landau damping.

After a while, le mode m=3 starts growing, which induces a second increase of m=6 (harmonics of m=3).

Further dynamics corresponds to an inverse cascade, Involving the successive amplification of the (m=2) backward and then (m=1) forward Alfvén modes.

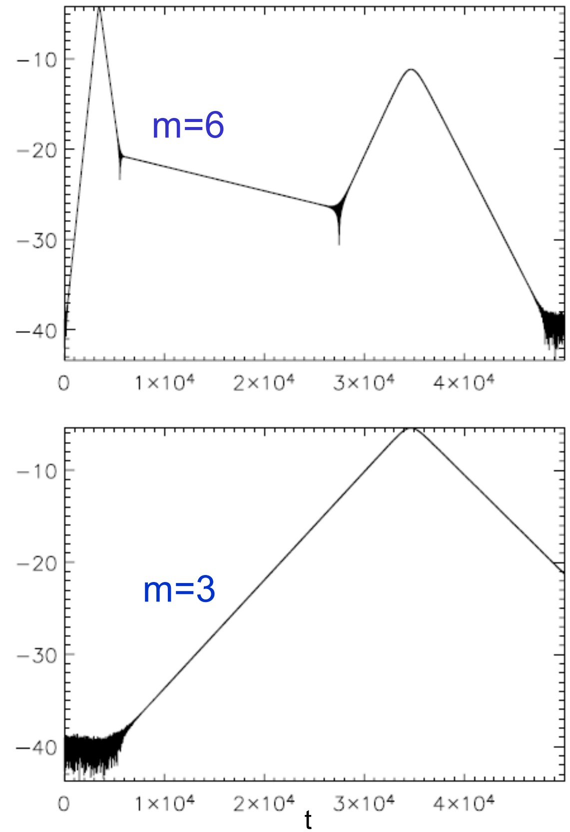

Fig. 4. Time evolution of the amplitude of the density modes $m=6$ (top) and $m=3$ (bottom) in lin-log scales, for a right-hand polarized Alfvén wave of amplitude $b_0=0.1$, $k_0=0.64$, in a plasma with $R_p=1$, $\beta=0.42$ and equal electron and ion equilibrium temperatures.

Zero electron temperature

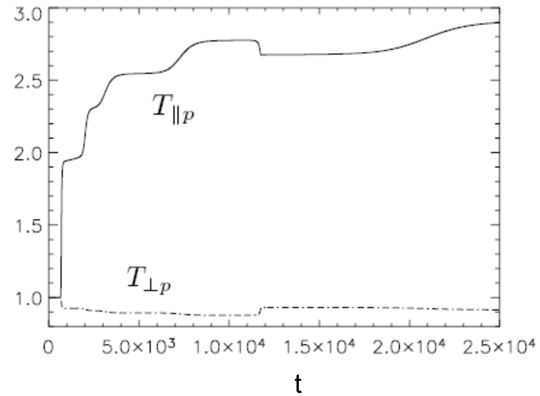

Fig. 5. Time evolution of the ion mean parallel (solid line) and perpendicular (dashed-dotted line) temperatures for a right-handed Alfvén wave with amplitude b_0=0.5, k_0=0.408, in a plasma with β=.45, R_p=1, and zero electron equilibrium temperature.

Electrons remain cold

Qualitative agreement with hybrid simulations (Vasquez 1995)

Modulational instability *(requires dispersion)*

(forward-propagating) left-hand polarized pump of amplitude $b_0=0.3$ and wavenumber $k_0=0.408=8\times 2\pi / D$ (D= 1 ion inertial length)
$\beta=1.5$, $T_e^{(0)}=2T_p^{(0)}$

t = 2000

t = 3500

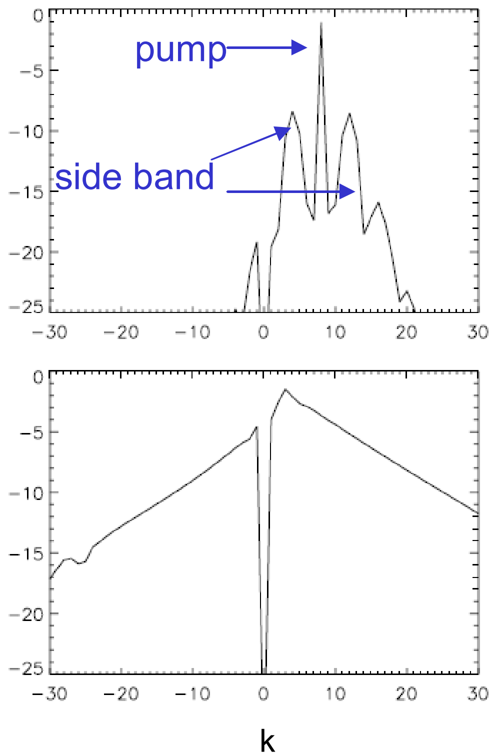

Fig. 7. Spectral density (versus the wavenumber index) in lin-log10 scale for the transverse magnetic field $b_+=b_x+ib_y$ at time $t=2000$ (top) and $t=3700$ (bottom) belonging, respectively, to the linear and nonlinear phases for the instability of a left-hand polarized Alfvén wave with amplitu and $T_e^{(0)}=2T_p^{(0)}$.408, in a plasma where $\beta=1.5$,

Confirm the prediction of Mjølhus and Wyller (1988), based on the *Kinetic Derivative NonLinear Schrödinger equation* (Rodinger 1971), obtained by a long wavelength reductive perturbation expansion from Vlasov Maxwell equations, that a small-amplitude, left-hand polarized Alfvén wave is modulationally instable for all β (Spangler 1989, 1990; Medvedev & Diamond 1996). This contrasts with fluid description.

Reductive perturbative expansion on dispersive Landau fluids reduces to KDNLS equation up to the approximation of the plasma response function by means of Padé approximants.

Modulational instability (nonlinear regime)

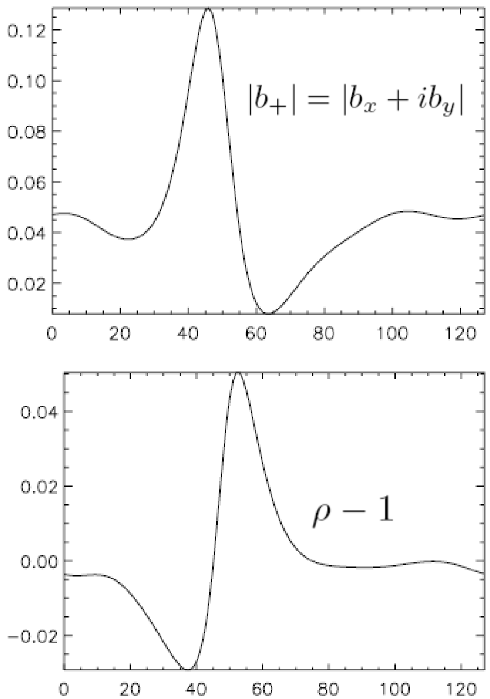

Fig. 8. Profile of $|b_+|^2$ (top) and $(\rho-1)$ (bottom) at t=3700 in the conditions of Fig. 7. The labels on the abscissa axis refer to the collocation point indices.

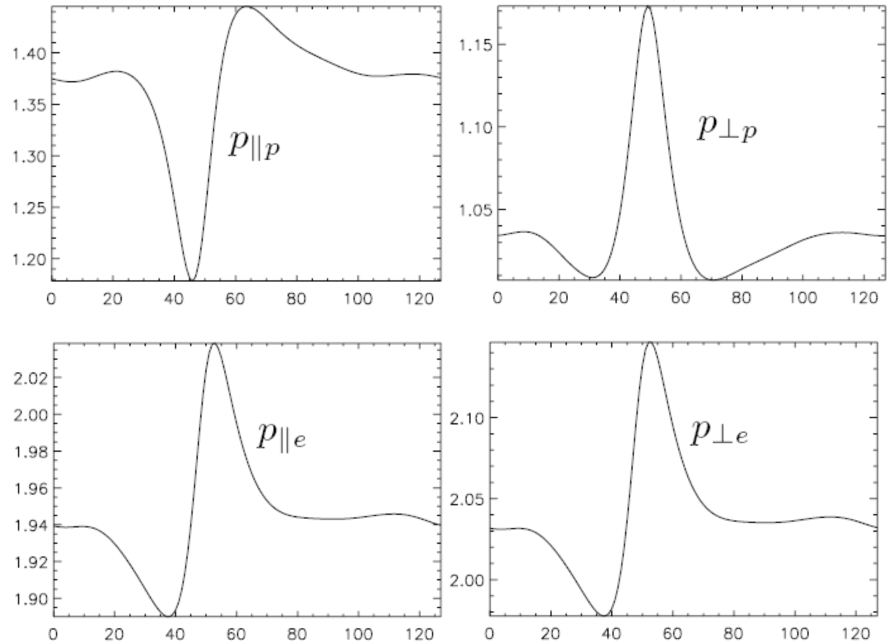

Fig. 9. Parallel (left) and transverse (right) pressures of the ions (top) and the electrons (bottom) at t=3700, in the conditions of Fig. 7. The labels on the abscissa axis refer to the collocation point indices.

Parallel and transverse electron pressures are proportional to the density variations.
This justifies the description of the electrons as an Isothermal fluid.

Modulational instability (continued)

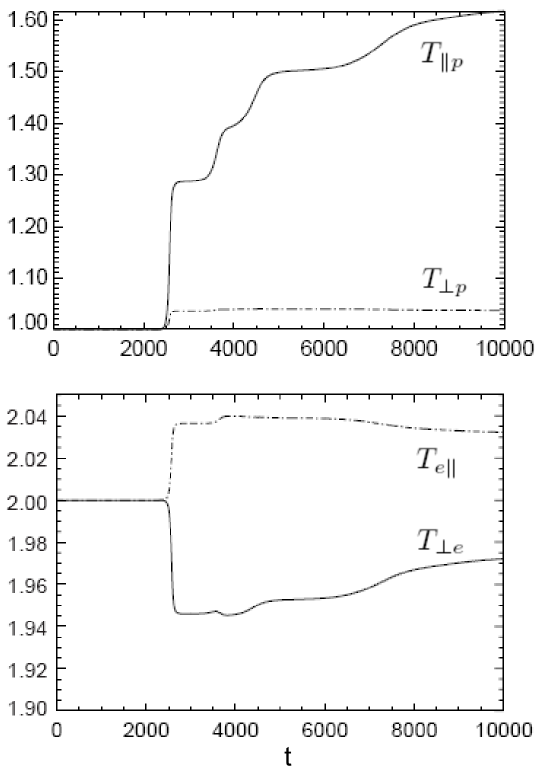

Fig. 10. Time evolution of parallel (solid lines) and transverse (dashed-dotted lines) of the ion (top) and electron (bottom) mean temperatures in the conditions of Fig. 7.

Presence of plateaux (with duration limited by onset of new dominant modes).

Dominant ion heating in the parallel direction

Some heating in the ions in the perpendicular direction (≠ cooling in the case of decay instability)

In brief:

perpendicular ion cooling

decay instability:

dominant parallel ion heating

modulational instability:

perpendicular ion heating

Filamentation instability: transverse modulational instability of Alfvén waves. Leads to formation of *magnetic filaments* (Shukla & Stenflo, 1989)

Requires dispersion: a simple fluid description : Hall-MHD

The instability turns out to be strongly sensitive to kinetic effects

Hall-MHD equations with a polytropic equation of state

$$\partial_t \rho + \nabla.(\rho \mathbf{u}) = 0$$

$$\rho(\partial_t \mathbf{u} + \mathbf{u}.\nabla \mathbf{u}) = -\frac{\beta}{\gamma}\nabla \rho^\gamma + (\nabla \times \mathbf{b}) \times \mathbf{b}$$

$$\partial_t \mathbf{b} - \nabla \times (\mathbf{u} \times \mathbf{b}) = -\frac{1}{R_i}\nabla \times (\frac{1}{\rho}(\nabla \times \mathbf{b}) \times \mathbf{b})$$

$$\nabla.\mathbf{b} = 0$$

velocity unit: Alfvén speed
length unit : $R_i \times$ ion inertial length
time unit: $R_i \times$ ion gyroperiod
density unit: mean density
magnetic field unit: ambient field

Exact solutions: (Dispersive) Alfvén waves propagating along the ambient field

Filamentation of a LH plane polarized Alfvén wave

$\beta = 1.5$

Hall-MHD simulation

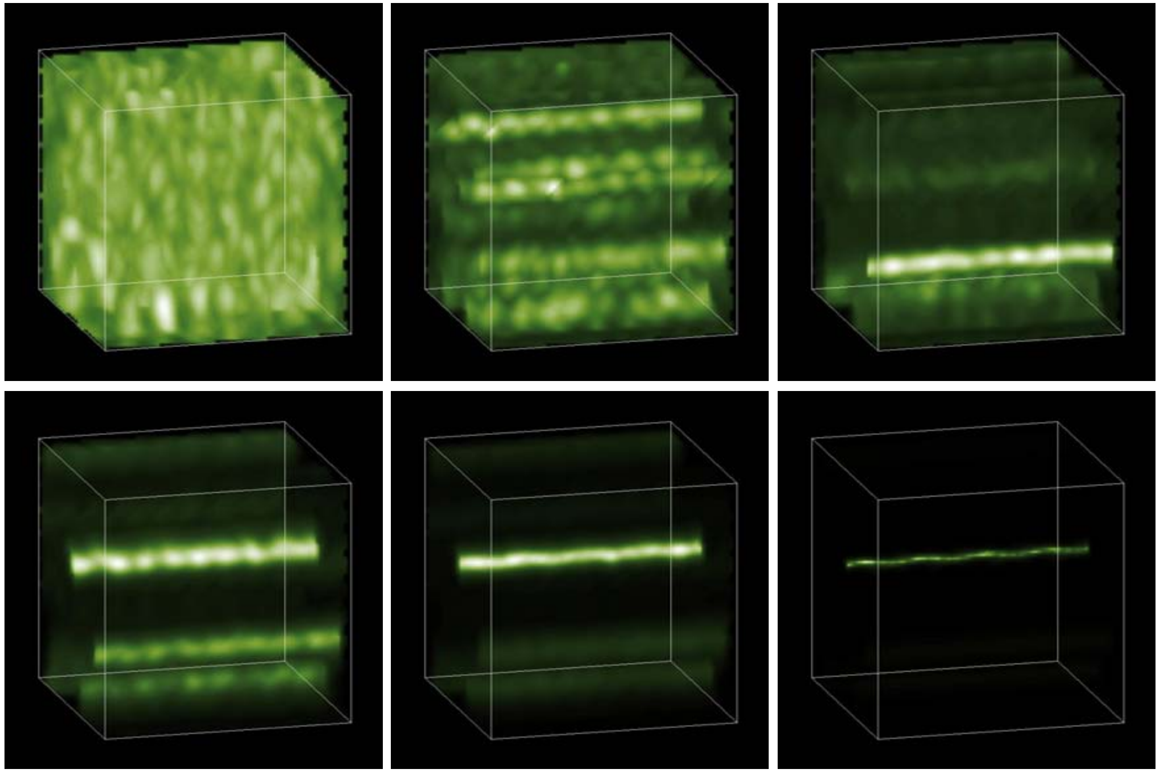

Direct numerical simulations of 3D Hall MHD (Laveder, Passot & Sulem Phys. Plasmas **9**, 293 (2002)).

(Laveder et al., Physica D,184, 237, 2003)

Initial conditions: circularly polarized Alfvén wave perturbed at large scales

Large-scale transverse modulation of a small-amplitude parallel Alfvén wave, amenable of a multiple-scale asymptotics

$$\boxed{i\partial_t B + \alpha \Delta_\perp B - k v_g \left(\frac{1}{v_g^2} - \frac{k^4}{4(\beta+1)\omega^4} \right) |B|^2 B = 0,}$$

Champeaux, Passot & Sulem, JPP **58**, 665 (1997)

$$v_g = \omega' = \frac{2\omega^3}{k(k^2+\omega^2)}$$

$$\alpha = \left(\frac{k\omega}{k^2+\omega^2} \right) \left(\frac{\omega^2}{2k^3} - \frac{\beta k}{2(\beta k^2 - \omega^2)} \right)$$

Note that $\alpha \neq \dfrac{v_g}{2k}$

B denotes the complex amplitude of the pump, defined by $b_y + i\sigma b_z = B \exp i(kx - \omega t)$

$$\omega = -\frac{\sigma}{2R_i} k^2 + k\sqrt{1 + \frac{k^2}{4R_i^2}}$$

σ= +1 or -1 depending on the RH or LH polarization of the wave.

Instability when coefficients of diffraction and of the nonlinear coupling coefficient have the same sign.

In the long-wavelength limit, filamentation instability for $\beta > 1$

The conditions for filamentation instability are strongly affected by kinetic effects

(Passot & Sulem, Phys. Plasmas 10, 3887, 2003)

Reductive perturbative expansion performed from ***Vlasov-Maxwell equations*** leads to a multidimensional Kinetic Derivative NonLinear Schrödinger equation for the Alfvén wave amplitude, coupled to a dynamical equation for a mean field including several contributions (among them the parallel velocity and magnetic field)

A (transverse) modulational analysis then leads to the dissipative 2D NLS equation

$$i\partial_T\psi + \frac{B_0}{2\lambda\rho^{(0)}}(P_1 + iP_2)\Delta_\perp\psi - k\langle U\rangle\psi = 0,$$

that includes a linear diffusive term associated with Landau damping, in addition to the diffraction and to the potential <U> to be determined in terms of ψ.

When linearly perturbing a plane wave solution ψ_0

with harmonic perturbations of wavenumber K and frequency Ω, one gets the dispersion relation

$$\Omega = i\nu K^2 \pm \sqrt{2C_1\chi k\lambda\frac{|\psi_0|^2}{B_0^2}K^2 + \chi^2K^4}.$$

For bi-Maxwellian plasma, $\nu < 0$

For a plasma fire-hose stable, $C_1 > 0$

Filamentation instability when $\chi_* \equiv 1 + \beta_\perp + \frac{K_1}{\rho^{(0)}v_A^2} < 0.$

K_1 coefficient associated with Landau damping.

Filamentation instability when $\chi_* < 0$

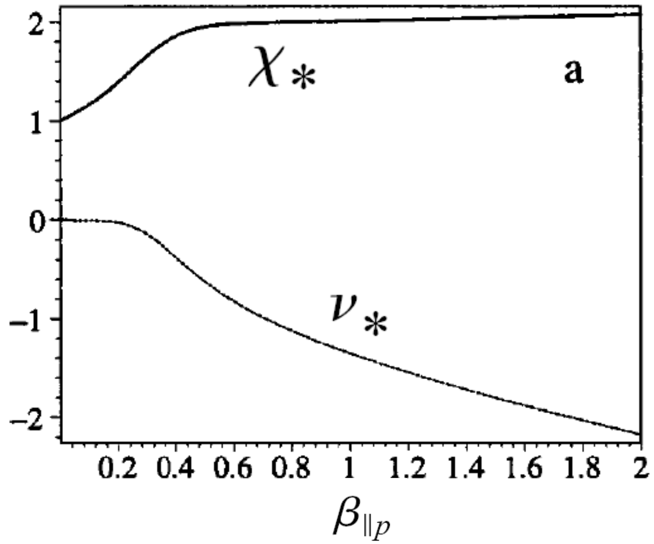

Examples:

1) Equal and isotropic proton and electron temperatures
   No filamentation instability

2) Isotropic ion and electron temperatures with equilibrium temperature ratio T_e/T_p =8

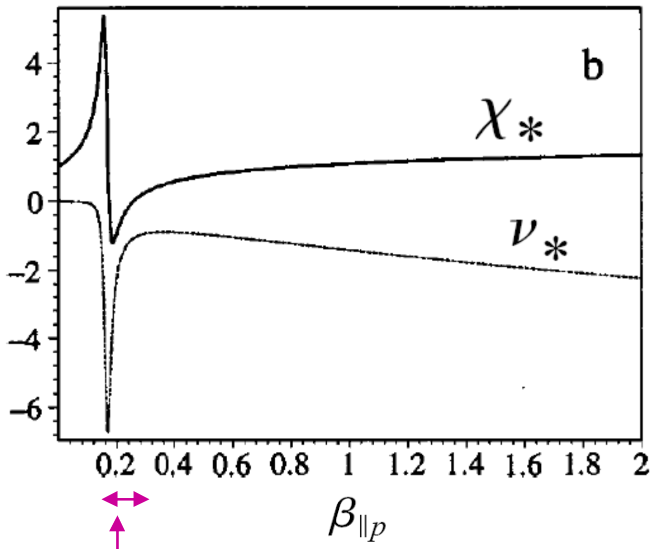

Filamentation instability
(theory)

Temperature anisotropy extends
the instability range

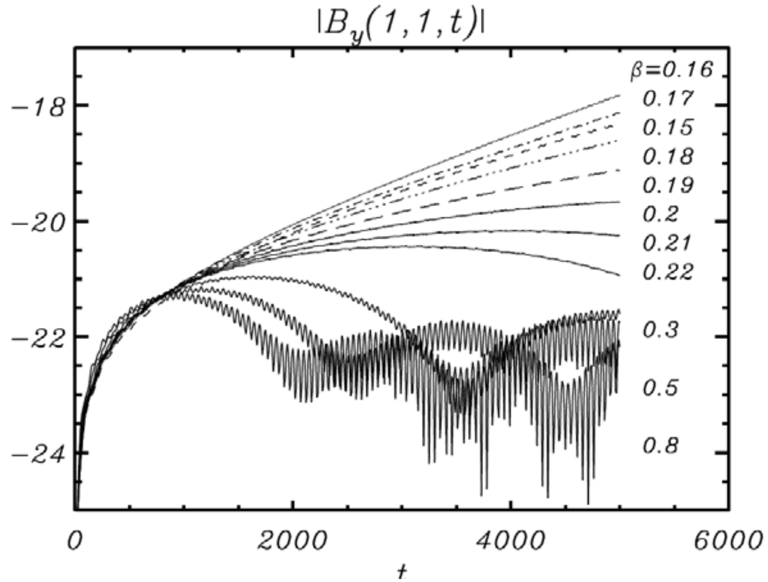

Landau fluid simulations
(with D. Borgogno)

Landau damping leads to an early saturation of the instability, leading to magnetic filaments of very small intensity.

More significant amplification is observed in the presence of a density channel.

High density channel: formation of filaments of moderate intensity

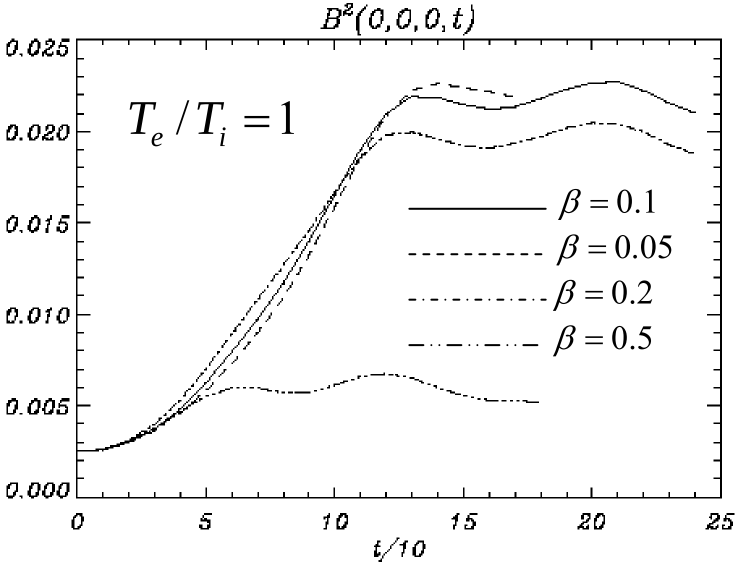

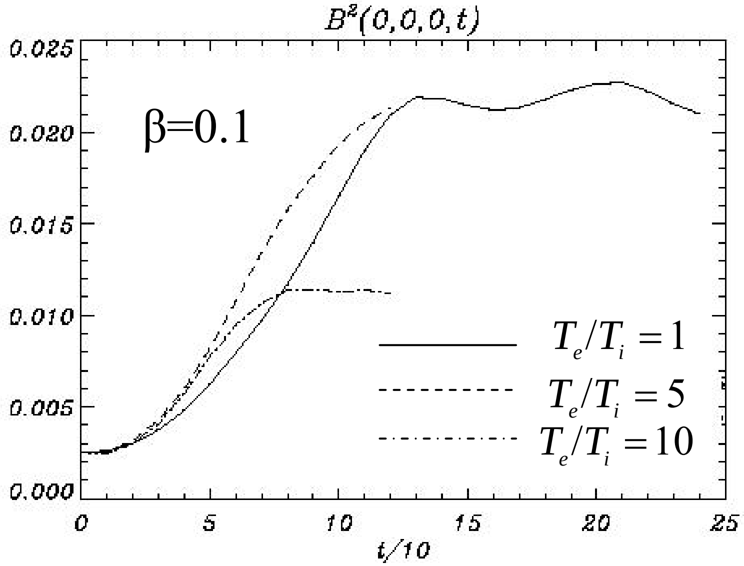

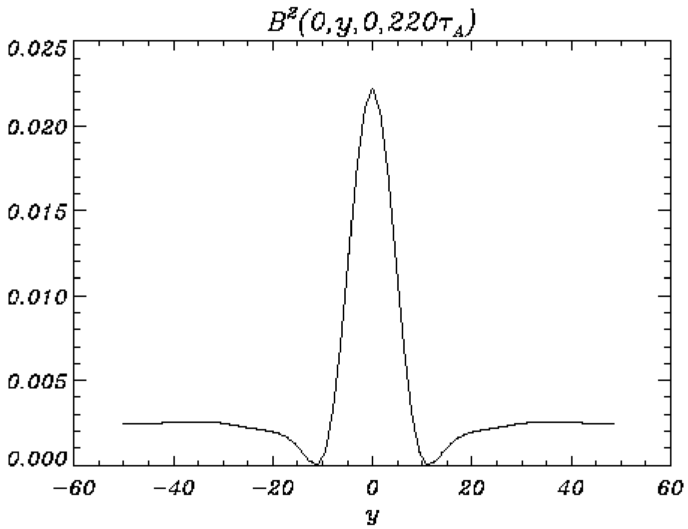

Transverse cut

β=0.1
$T_e/T_i=1$

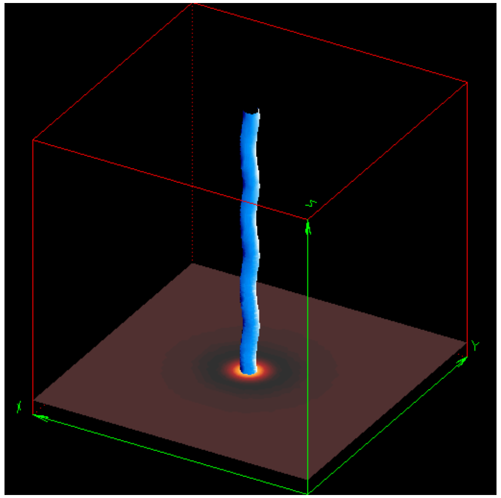

Mirror instability: Can occur in a plasma with anisotropic ion temperature $(T_{\perp p} > T_{\| p})$

Quasi-transverse near threshold ($\frac{T_\perp}{T_\|} - 1 > \frac{1}{\beta_\perp}$ for cold electrons)

Anisotropic ion cyclotron instability is not captured by low-frequency asymptotics.

The growth rate of mirror instability in the “quasi-hydrodynamic” limit is accurately captured by SHD Landau fluid model (in contrast with anisotropic MHD).

SHD: Snyder, Hammett & Dorland (1997)

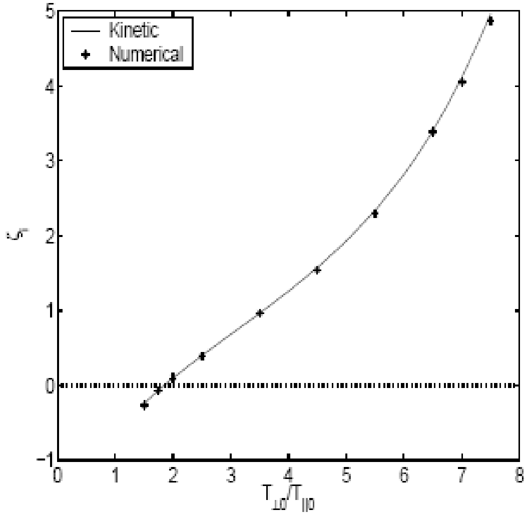

Figure 5: Mirror mode growth rate $\zeta_p = Im(\omega)/(k_z v_{\rm th})$ in a quasi-transverse direction $(\cot\theta = 0.01)$, predicted by the kinetic theory and given by time integration of the Landau fluid model, versus equilibrium temperature anisotropy for a plasma with $\beta = (2\beta_\perp + \beta_\|)/3 = 1$ and equal temperatures for electrons and protons.

Mirror instability extends to TRANSVERSE SCALES COMPARABLE TO ION LARMOR RADIUS. Such scales cannot be ignored.

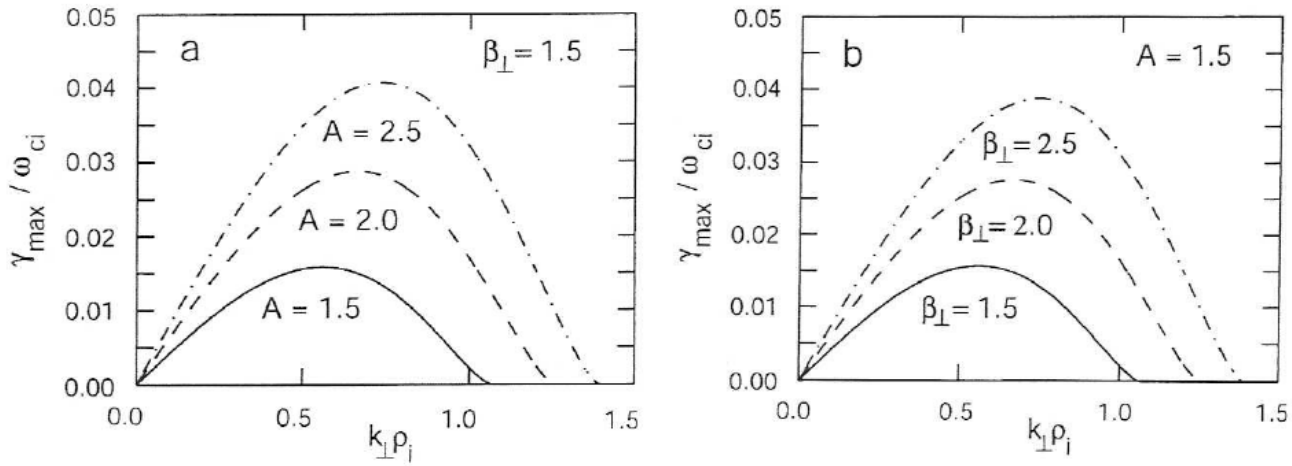

Instability growth rate versus the transverse wavenumber for various $\beta_{\perp p}$ and anisotropy factor $A = T^{(0)}_{\perp p}/T^{(0)}_{\| p} - 1$ [From Pokhotelov et al. (2004) JGR **109**, A09213].

In the quasi-hydrodynamic approach, maximum growth rate proportional to $k_\perp r_L$, whereas kinetic theory predicts a quenching of the instability for perpendicular scales of the order of the ion Larmor radius.

Retaining only the large scales leads to an ill-posed problem (the smallest retained scales are the most unstable).

FLR effects at SMALL transverse scales should be retained to reproduce the quenching of the mirror instability.

II. Retaining small quasi-transverse scales (gyrokinetic scaling)

Finite Larmor radius effects:

Gyroviscous tensor: $\overline{\overline{\mathbf{\Pi}}} = \overline{\overline{\mathbf{\Pi}}}_\perp + \Pi_\| \otimes \widehat{b} + \widehat{b} \otimes \Pi_\|$

It is convenient to write $\quad \frac{1}{p^{(0)}_{\perp p}} \nabla_\perp \cdot \overline{\overline{\mathbf{\Pi}}}_\perp = -\nabla_\perp \mathcal{A} + \nabla_\perp \times (\mathcal{B}\widehat{z}).$

By combining expressions of the various fields provided by the kinetic theory in order to eliminate the plasma response function, one gets

$$\mathcal{A} = \left[1 - \frac{\Gamma_1(b)}{b[\Gamma_0(b) - \Gamma_1(b)]} + \frac{\Gamma_1(b)}{\Gamma_0(b)}\right] \frac{1}{\Omega}(ik_\perp \times u_{\perp p}) \cdot \widehat{z} - \frac{\Gamma_1(b)}{\Gamma_0(b)} \frac{T^{(1)}_{\perp p}}{T^{(0)}_{\perp p}}$$

$$\mathcal{B} = -\left[\frac{\Gamma_0(b) - 1 - \Gamma_1(b)}{b} + 2(\Gamma_0(b) - \Gamma_1(b)) + \frac{\Gamma_0(b) - \Gamma_1(b)}{1 - \Gamma_0(b)}(\Gamma_0(b) - \Gamma_1(b) - \frac{1 - \Gamma_0(b)}{b})\right]$$
$$\times \frac{c}{\Omega B_0}(ik_\perp \times E_\perp) \cdot \widehat{z} + \frac{1}{1 - \Gamma_0(b)}\left[\Gamma_0(b) - \Gamma_1(b) - \frac{1 - \Gamma_0(b)}{b}\right] \frac{1}{\Omega}(ik_\perp \cdot u_{\perp p}).$$

In the large scale limit $b = \dfrac{k_\perp^2}{\Omega^2} \dfrac{T^{(0)}_{\perp p}}{m_p} \to 0$, the usual fluid estimates are recovered:

$$\mathcal{A}_{fluid} = \tfrac{1}{2\Omega}(\nabla_\perp \times u_\perp) \cdot \widehat{z}, \quad \mathcal{B}_{fluid} = \tfrac{1}{2\Omega}(\nabla_\perp \cdot u_\perp)$$

In order to reproduce the leading-order nonlinear fluid theory, replace $p^{(0)}_{\perp p}$ by $p_{\perp p}$ (averaged on the domain)

T. Passot & P.L. Sulem, Phys. Plasmas 14, 082502 (2007)

Validation of the FLR –Landau fluid model by comparison with the linear kinetic theory

Mirror modes

Comparison FLR-Landau fluid (+) with kinetic theory (——)

Normalized growth rate ω_i/Ω_p versus $k_\perp r_L$

$\tau = T_{\parallel e}/T_{\parallel p}$

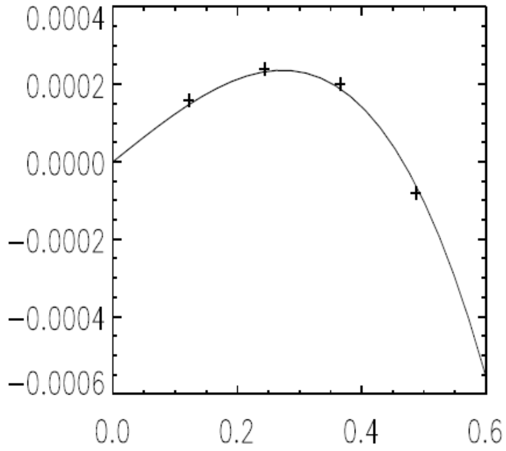

$\beta = 5$, $\tau = 0.1$, $\theta = \cos^{-1}(.1)$,
$T_{\perp p}/T_{\parallel p} = 1.2$ and $T_{\perp e}/T_{\parallel e} = 1.$

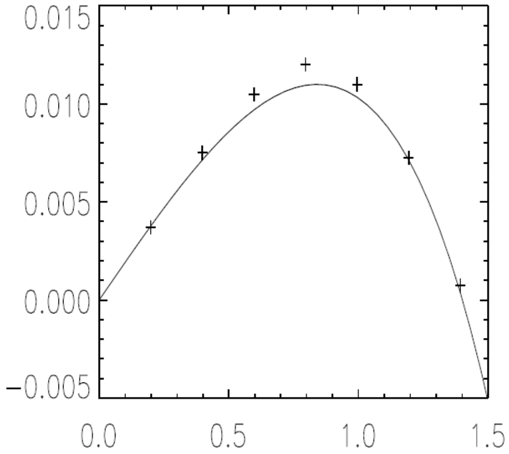

$\beta = 2$, $\tau = 1$, $\theta = \cos^{-1}(.1)$,
$T_{\perp p}/T_{\parallel p} = 2$ and $T_{\perp e}/T_{\parallel e} = 1.$

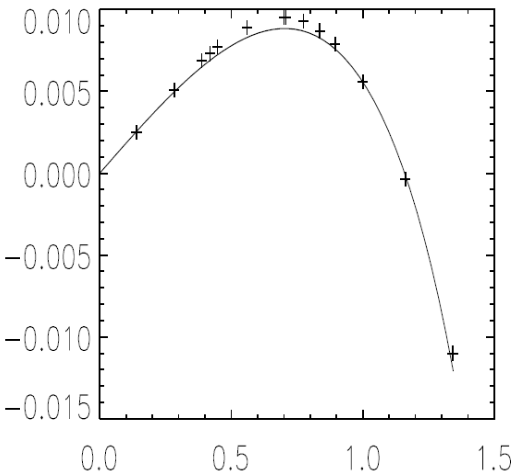

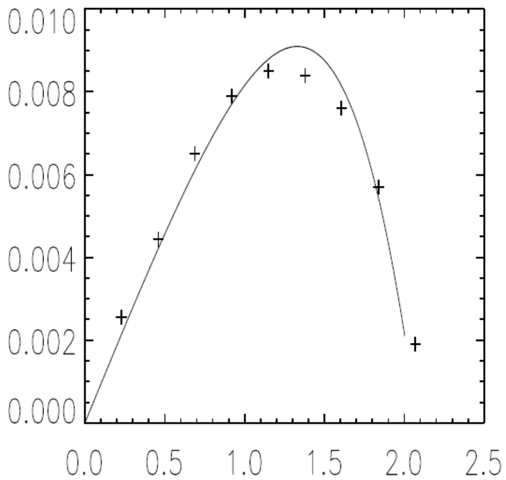

$\beta = 5$, $\tau = 1$, $\theta = \cos^{-1}(.2)$,

$T_{\perp p}/T_{\parallel p} = 1.4$ and $T_{\perp e}/T_{\parallel e} = 1.$

$T_{\perp p}/T_{\parallel p} = 1.1$ and $T_{\perp e}/T_{\parallel e} = 1.18$

Kinetic Alfvén waves

quasi-transverse propagation

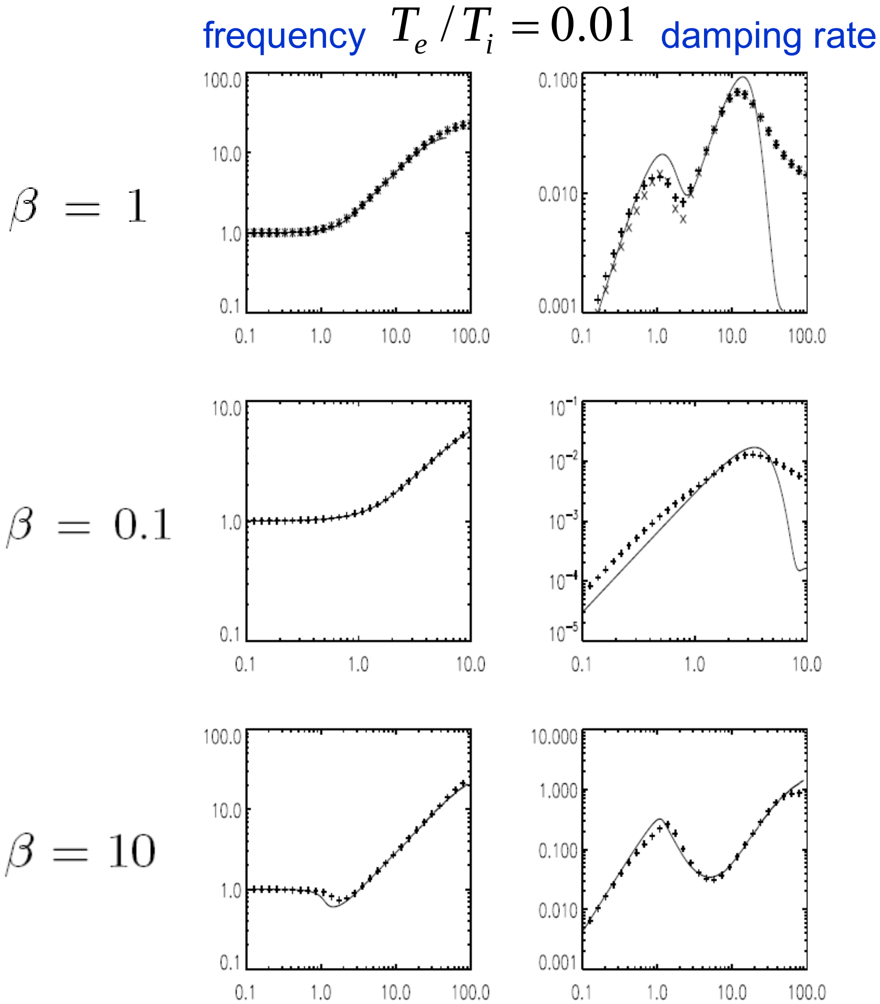

FIG. 1: Normalized frequency $\omega_r/(k_\parallel v_A)$ (left) and damping rate $-\omega_i/(k_\parallel v_A)$ (right) for KAWs with $\theta = \tan^{-1}(1000)$, $\tau = 10^{-2}$, versus $k_\perp r_L$ for $\beta = 1$ (top), $\beta = 0.1$ (middle), $\beta = 10$ (bottom).

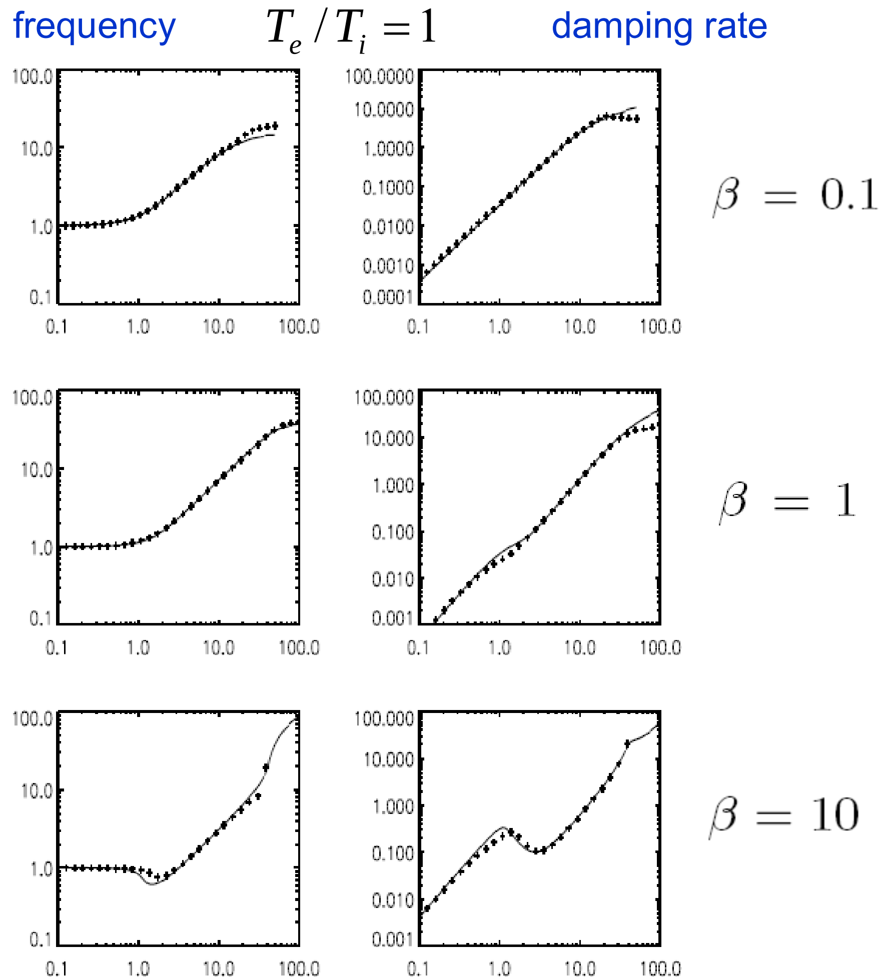

FIG. 2: Normalized frequency $\omega_r/(k_\parallel v_A)$ (left) and damping rate $-\omega_i/(k_\parallel v_A)$ (right) for KAWs with $\theta = \tan^{-1}(1000)$, $\tau = 1$, versus $k_\perp r_L$ for $\beta = 0.1$ (top), $\beta = 1$ (middle), $\beta = 10$ (bottom).

Alfvén waves

$\beta = 1$

oblique propagation

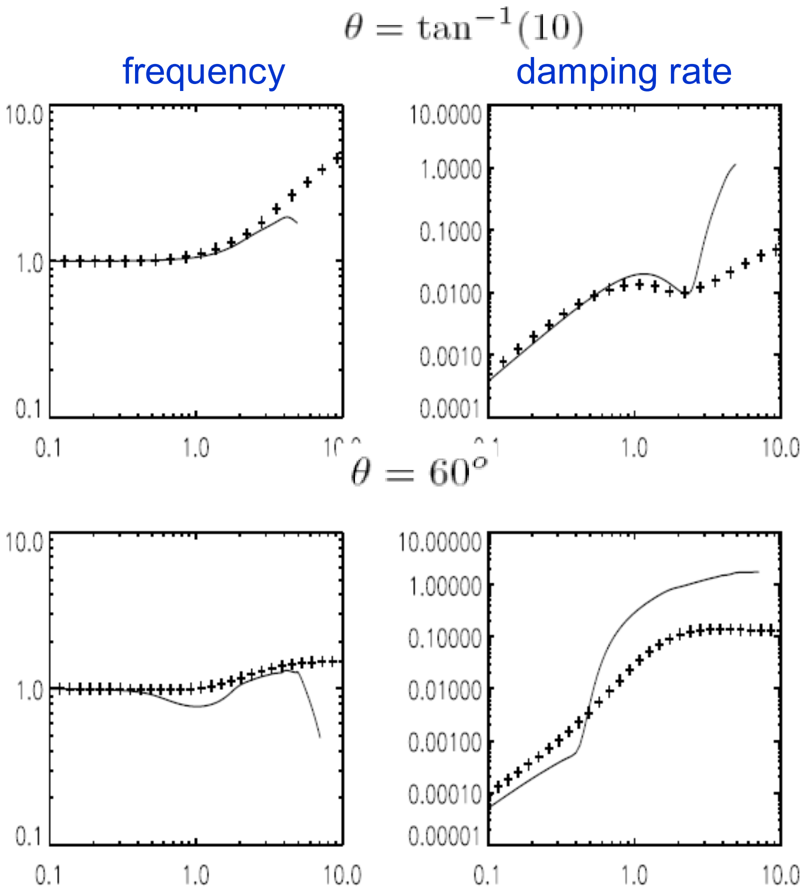

FIG. 3: Normalized frequency $\omega_r/(k_\parallel v_A)$ (left) and damping rate $-\omega_i/(k_\parallel v_A)$ (right) for KAWs with $\tau = 0.01$, $\beta = 1$ versus $k_\perp r_L$ for $\theta = \tan^{-1}(10)$ (top), $\theta = 60^o$ (bottom).

quasi-parallel propagation

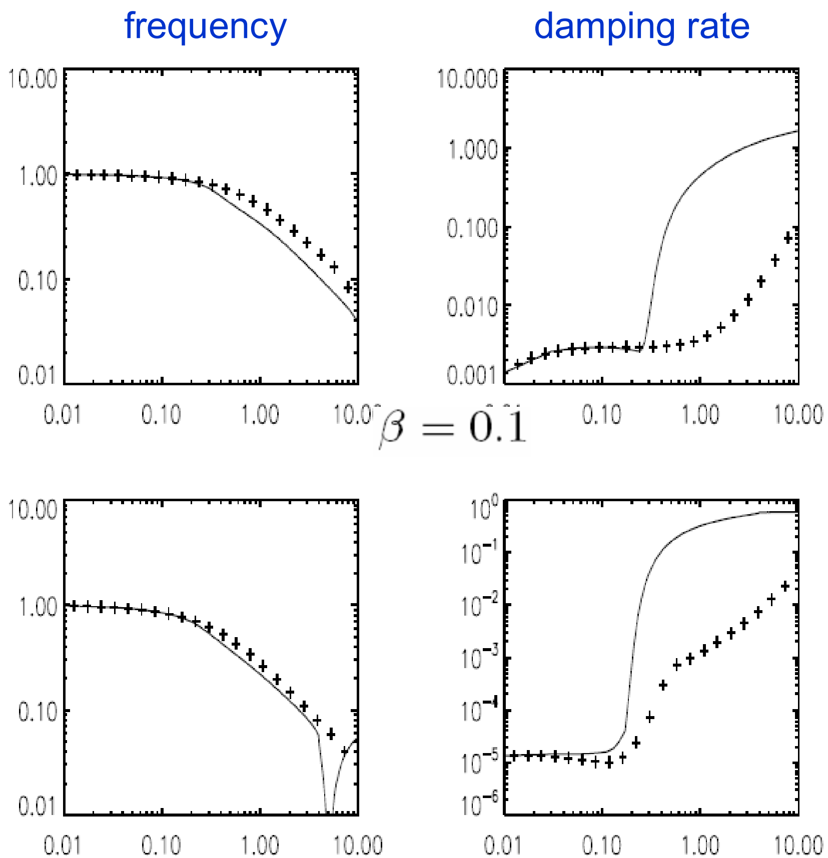

FIG. 4: Normalized frequency $\omega_r/(k_\parallel v_A)$ (left) and damping rate $-\omega_i/(k_\parallel v_A)$ (right) for AWs with $\tau = 1$, $\theta = \tan^{-1}(0.1)$, versus kr_L for $\beta = 1$ (top), $\beta = 0.1$ (bottom).

Slow waves

$\beta = 0.01$

Fast waves

frequency damping rate

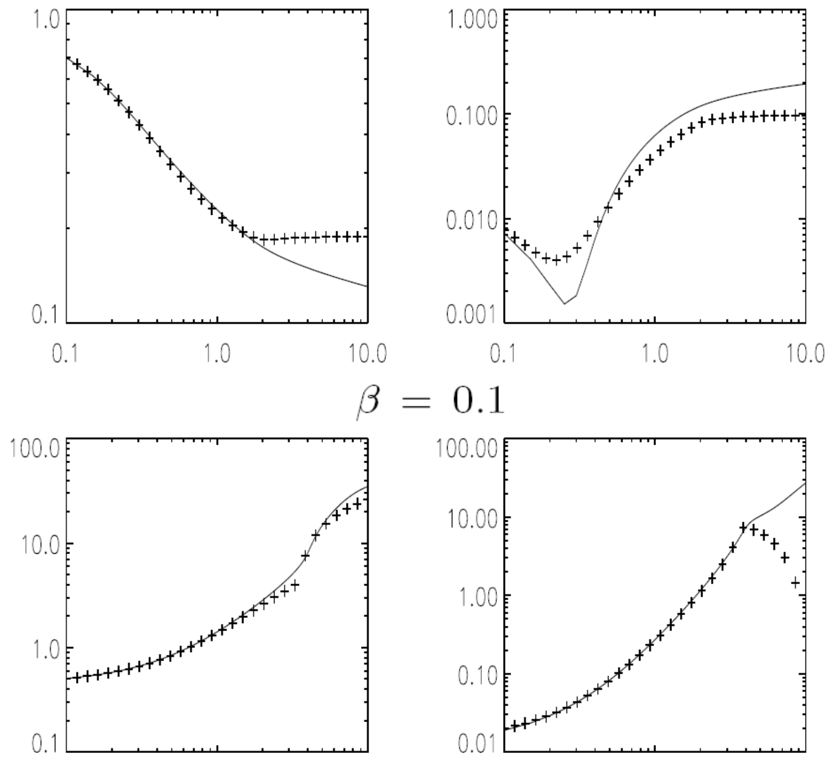

FIG. 5: Normalized frequency $\omega_r/(k_\parallel c_s)$ (left) and damping rate $-\omega_i/(k_\parallel c_s)$ (right) for slow waves with $\tau = 100$, $\theta = \tan^{-1}(1000)$ versus $k_\perp \rho_L$ for $\beta = 0.01$ (top), $\beta = 0.1$ (bottom).

frequency damping rate

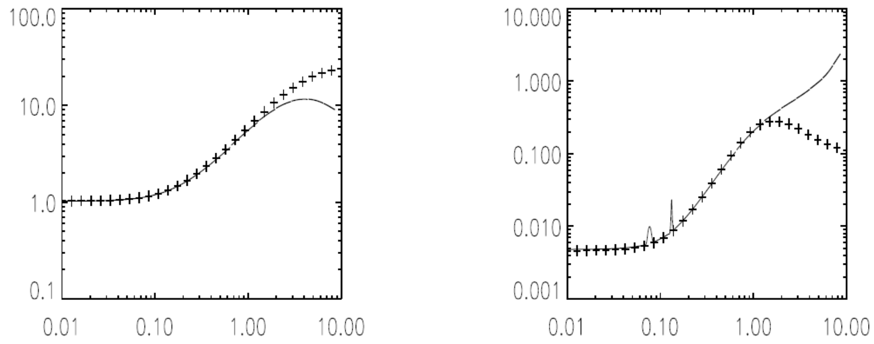

FIG. 7: Normalized frequency $\omega_r/(kv_A)$ (left) and damping rate $-\omega_i/(kv_A)$ (right) for fast waves with $\theta = 60^o$, $\tau = 10$, versus $k_\perp r_L$ for $\beta = 0.01$.

Nonlinear regime

- Nonlinear mirror modes
- Cascades of kinetic Alfvén waves

Nonlinear Mirror modes

Nonlinear dynamics of mirror modes is hardly amenable to a fluid-like description, even when linear kinetic effects are retained.

Nonlinear kinetic effects, including distortion of the space averaged distribution function, seem relevant.

Some aspects of mirror structures are nevertheless qualitatively reproduced.

from initial random noise $\quad T_{//e}/T_{//p} = 0.05, \quad T_{\perp e}/T_{//e} = 1, \quad \cos\theta = 0.2$

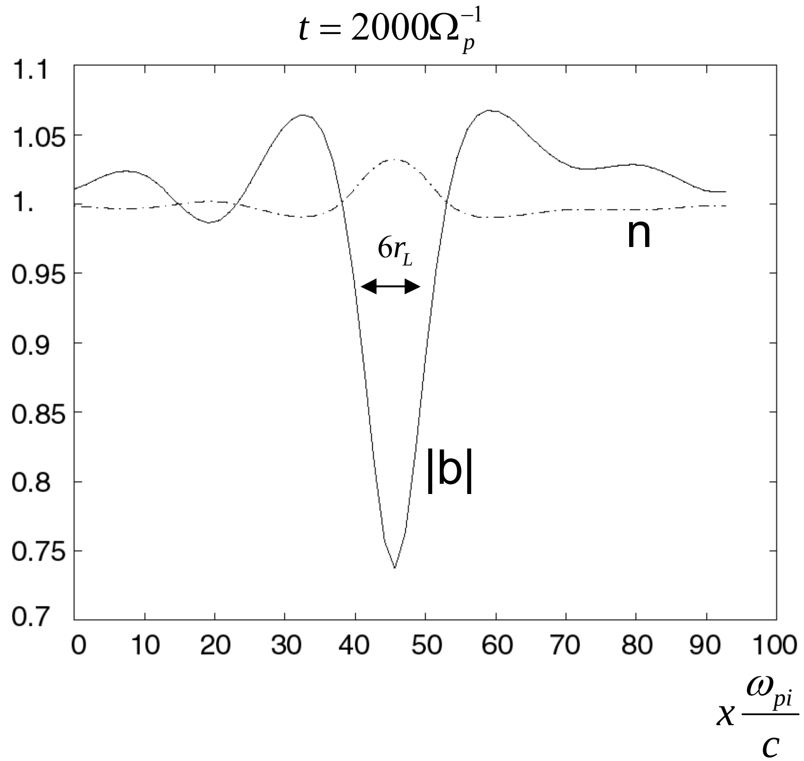

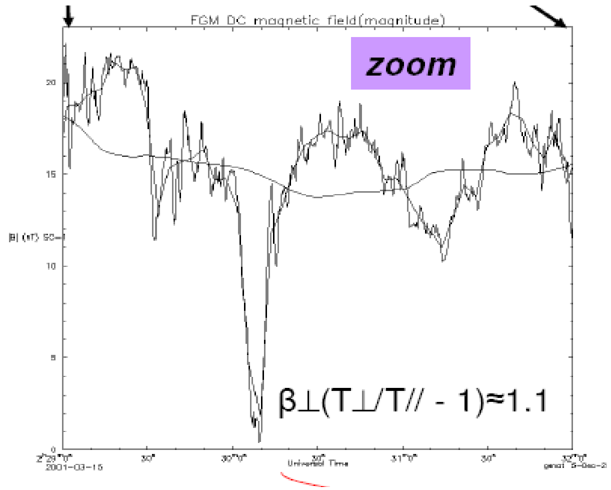

Cluster observations
(Génot et al. 2008)

Formation of quasi-static magnetic holes

$$\beta_{//p} = 5, \quad T_{\perp p}/T_{//p} = 1.5$$

The depth of the hole slowly decreases in time

from initial random noise

$t = 850\Omega_p^{-1}$

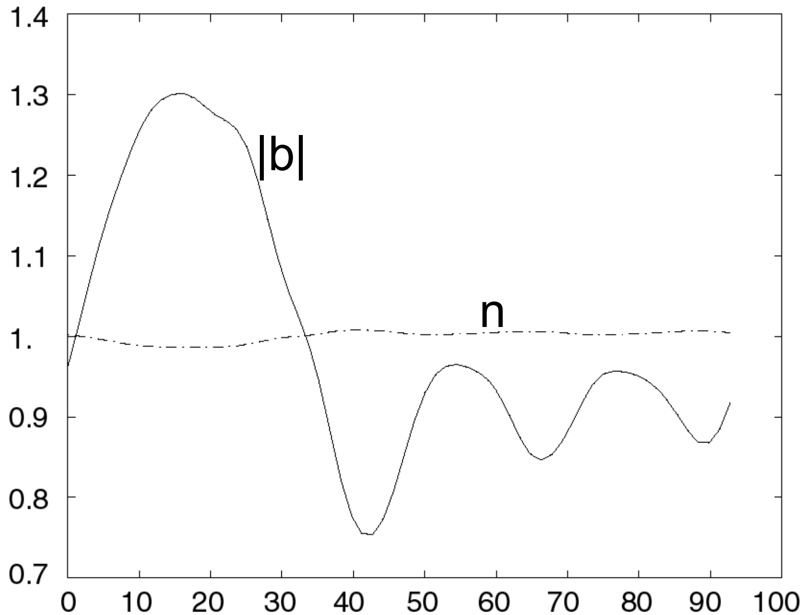

$x\dfrac{\omega_{pi}}{c}$

$$\beta_{//p} = 20, \quad T_{\perp p}/T_{//p} = 1.4$$
$$T_{//e}/T_{//p} = 0.05, \quad T_{\perp e}/T_{//e} = 1, \quad \cos\theta = 0.2$$

Formation of magnetic humps

At long times the peak amplitude is observed to decrease and a hole eventually forms.

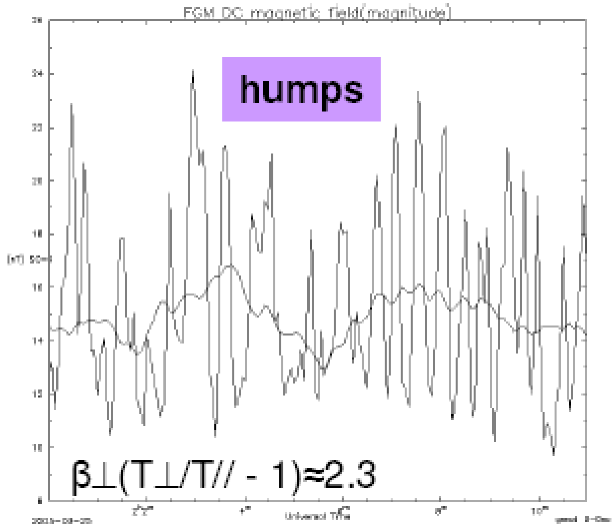

Cluster observations
(Génot et al. 2008)

Fixing mean proton temperatures

IC: random noise

(With D. Borgogno)

Simple way of imposing a forcing which, in real situations , is obtained through boundary conditions, such as for example an inflow.

In small domain: stationary solution

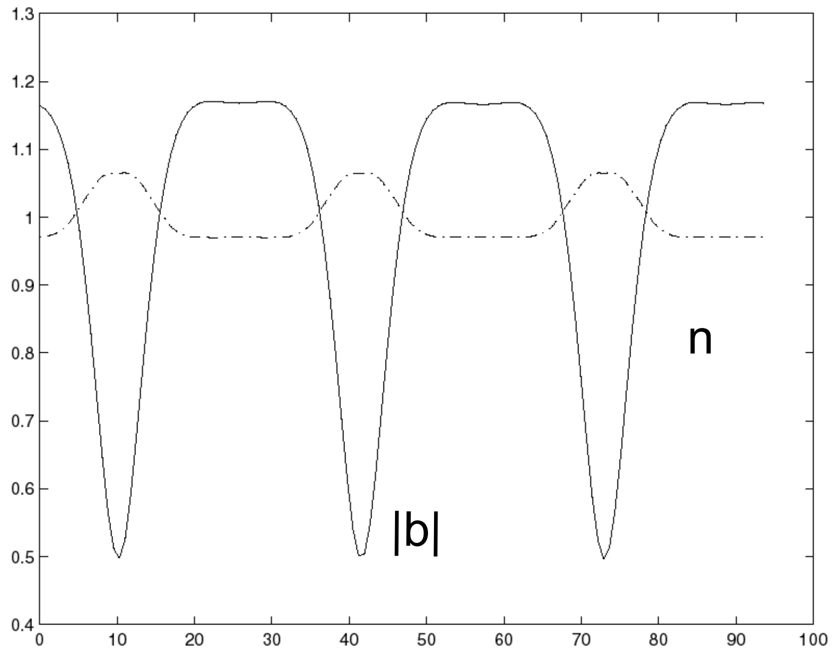

$$\beta_{//p} = 5, \quad T_{\perp p}/T_{//p} = 1.25$$

$$\cos\theta = 0.2$$

In large domains, these magnetic patterns are subject to spatio-temporal chaos

Presence of large-scale compression waves.

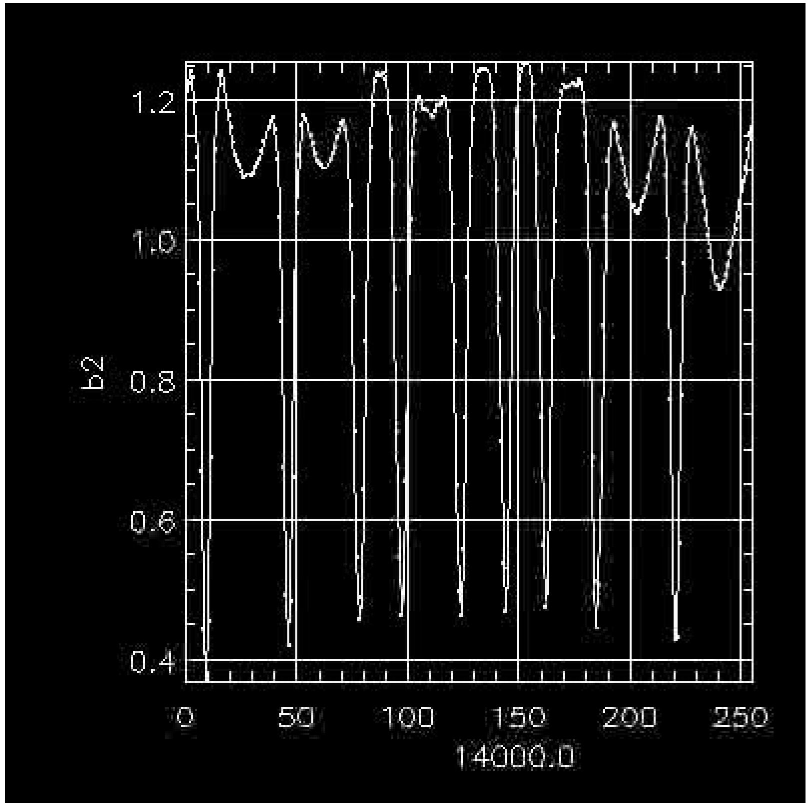

$$\cos\theta = 0.34 \qquad \beta_{//p} = 2, \quad T_{\perp p}/T_{//p} = 1.43$$

$$T_{//e}/T_{//p} = 0.05\,, \quad T_{\perp e}/T_{//e} = 1$$

Evidence of bistability

Stationary solution obtained by continuation below the threshold of mirror instability

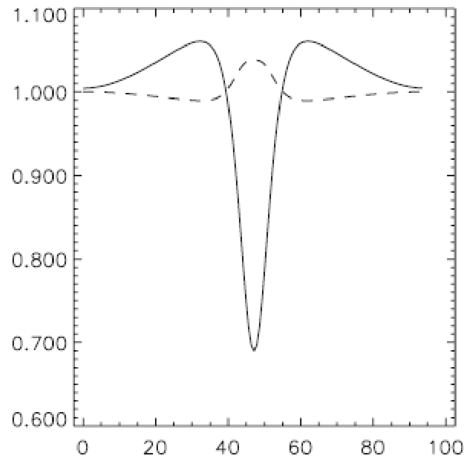

$\beta_{//p} = 5, \quad T_{\perp p}/T_{//p} = 1.25 \qquad \cos\theta = 0.2 \qquad T_{\perp e} = T_{\parallel e} = 0.05 T_{\parallel p}$

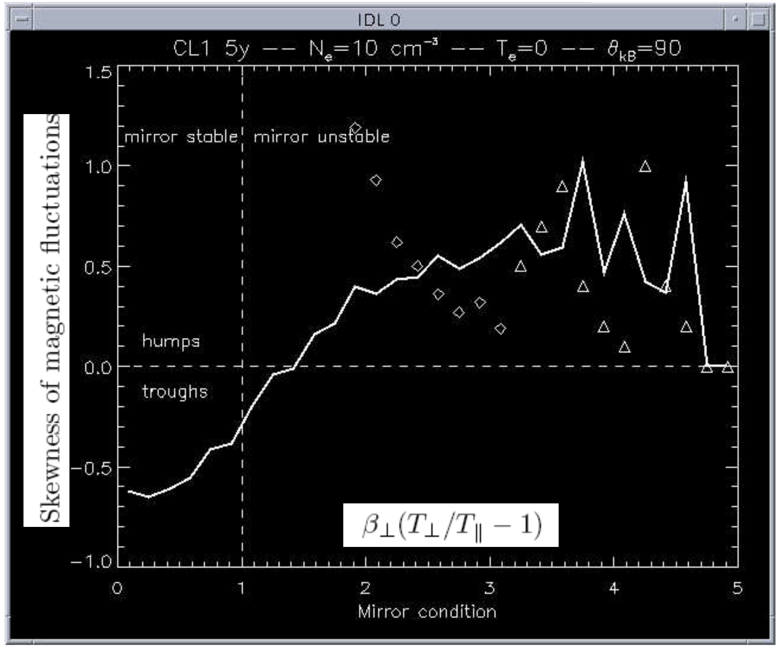

Statistics of structures observed in the magnetosheath

Courtesy of V. Génot.

Nonlinear Kinetic Alfvén waves

Kinetic Alfvén waves (and slow modes, but these ones are highly dissipative).
have been clearly identified using k-filtering technique by CLUSTER mission in the cusp region of the magnetosheath (Sahraoui et al. AIP **932**, 2007).

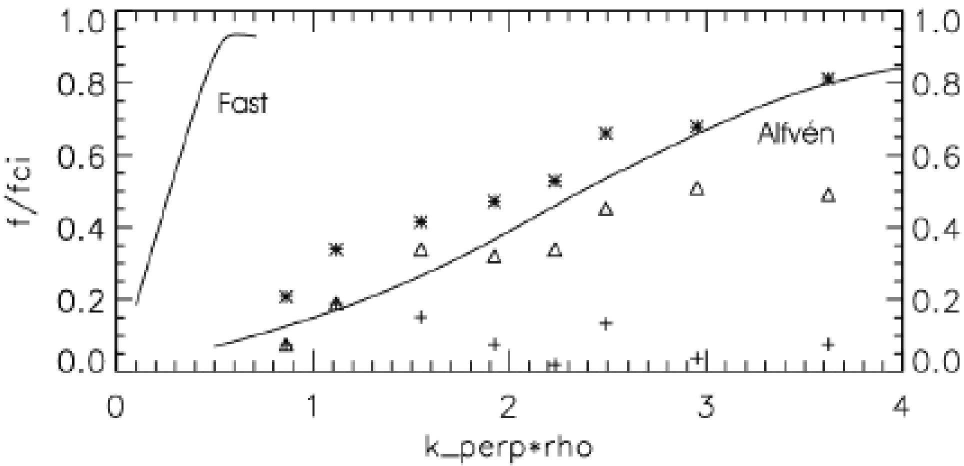

Another medium where KAWs play a fundamental role is the solar corona, where they are believed to mediate the conversion of large scale modes into heat.

Decay and cascades of kinetic Alfvén waves

Several regimes are observed

I. The initial wavelength is ***of the order or smalle*** than the ion gyroradius ρ_i with β=0.1, b_0 =0.02, θ=87,1°, $T_e/T_i=10^{-3}$, $k_{\perp 0}\, \rho_i$ =1.58.

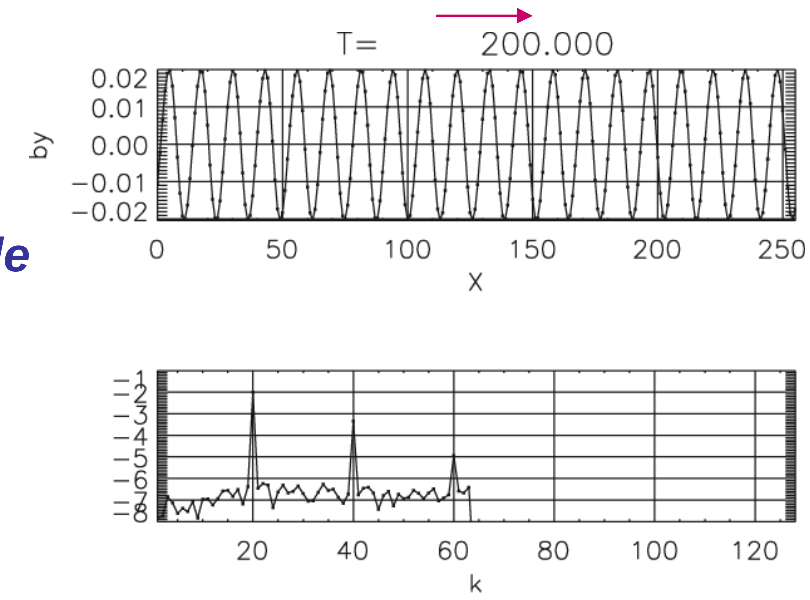

An instability develops (when $k_{\perp 0}\, \rho_i \geq 0.8$)
(growth rate increases with wave amplitude)

It is observed that:

- the magnetic energy spectrum increases for $k>k_0$
- the wave's amplitude slowly decays by Landau damping and nonlinear transfer.
- at the same time the wave slows down, stops and starts propagating backward with a very nonlinear profile.
- The parallel electron temperature increases but not the ion temperature.
- The perpendicular temperatures remain constant.

The problem need to be addressed with a Vlasov code to saturate the small-scale cascade.

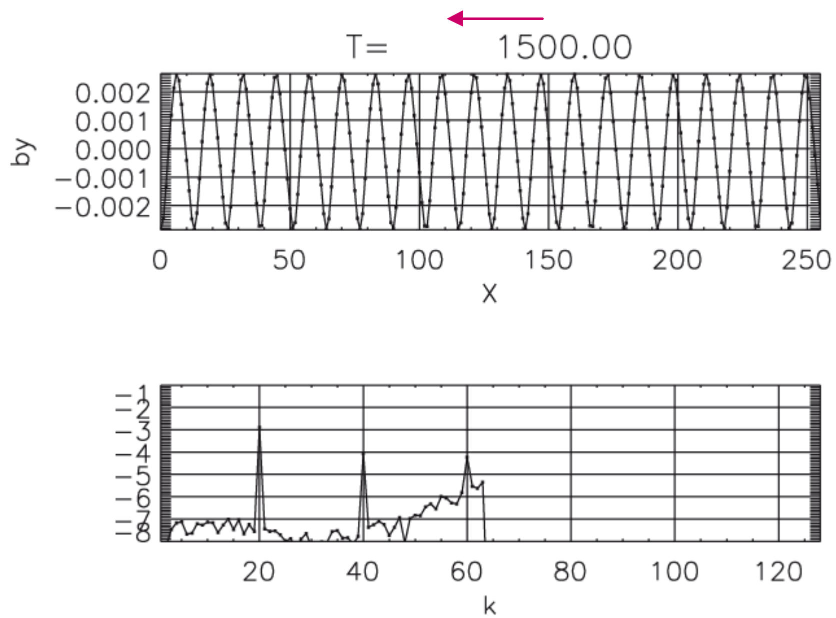

Growth rate of the high-k modes proportional to k.
(Small-scale kinetic effects missing ?)

II. The initial wavelength is much ***larger*** than the ion gyroradius with $\beta=0.01$, $b_0=0.1$, , $\theta=81{,}4^o$, $T_e/T_i=10^{-1}$

Choosing $k_{\perp 0}\,\rho_i=0.05$, we observe an inverse cascade characterized by:

- A bump in the spectrum corresponding to a slow drift of the wave mode and its satellites towards the smaller wavenumbers.

-The higher-k spectrum remains unchanged
- In physical space, the wave is a modulated train whose carrying wave gradually coarsens with alternating propagation directions.

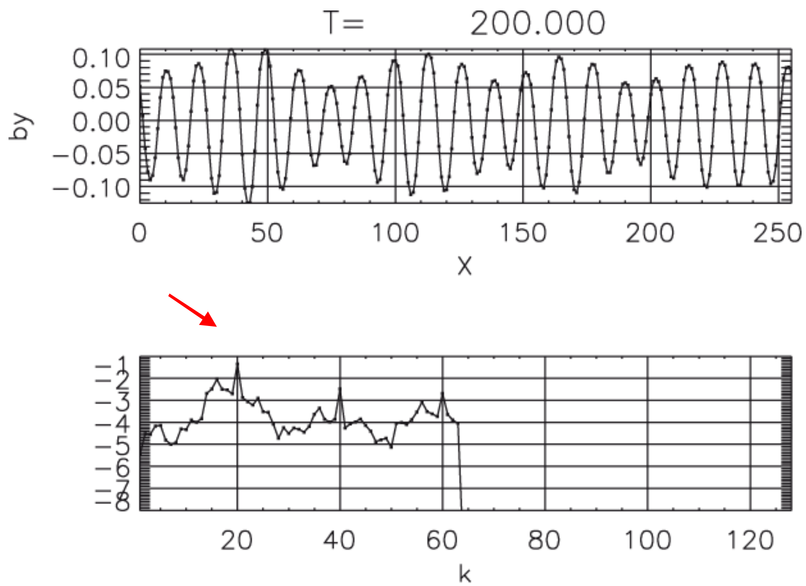

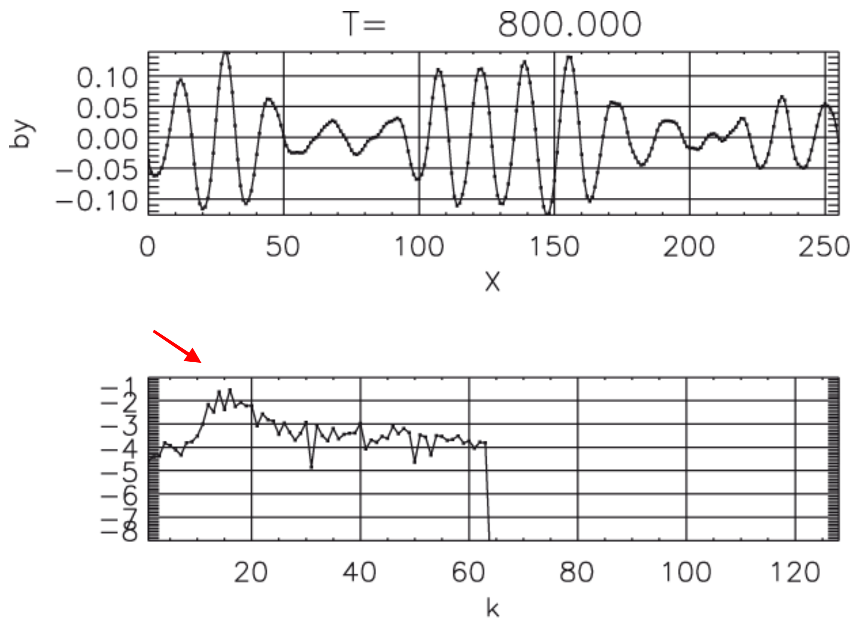

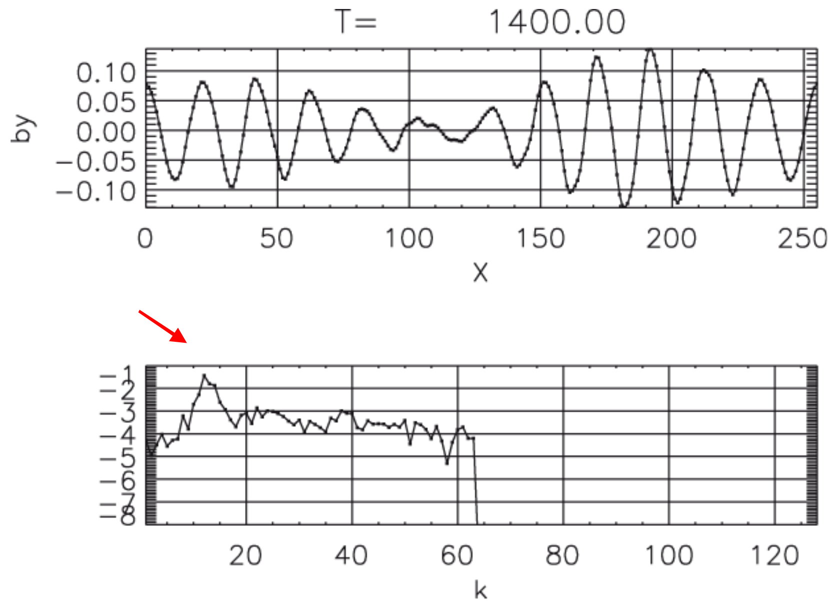

Times in unit of $5*\Omega_i^{-1}$

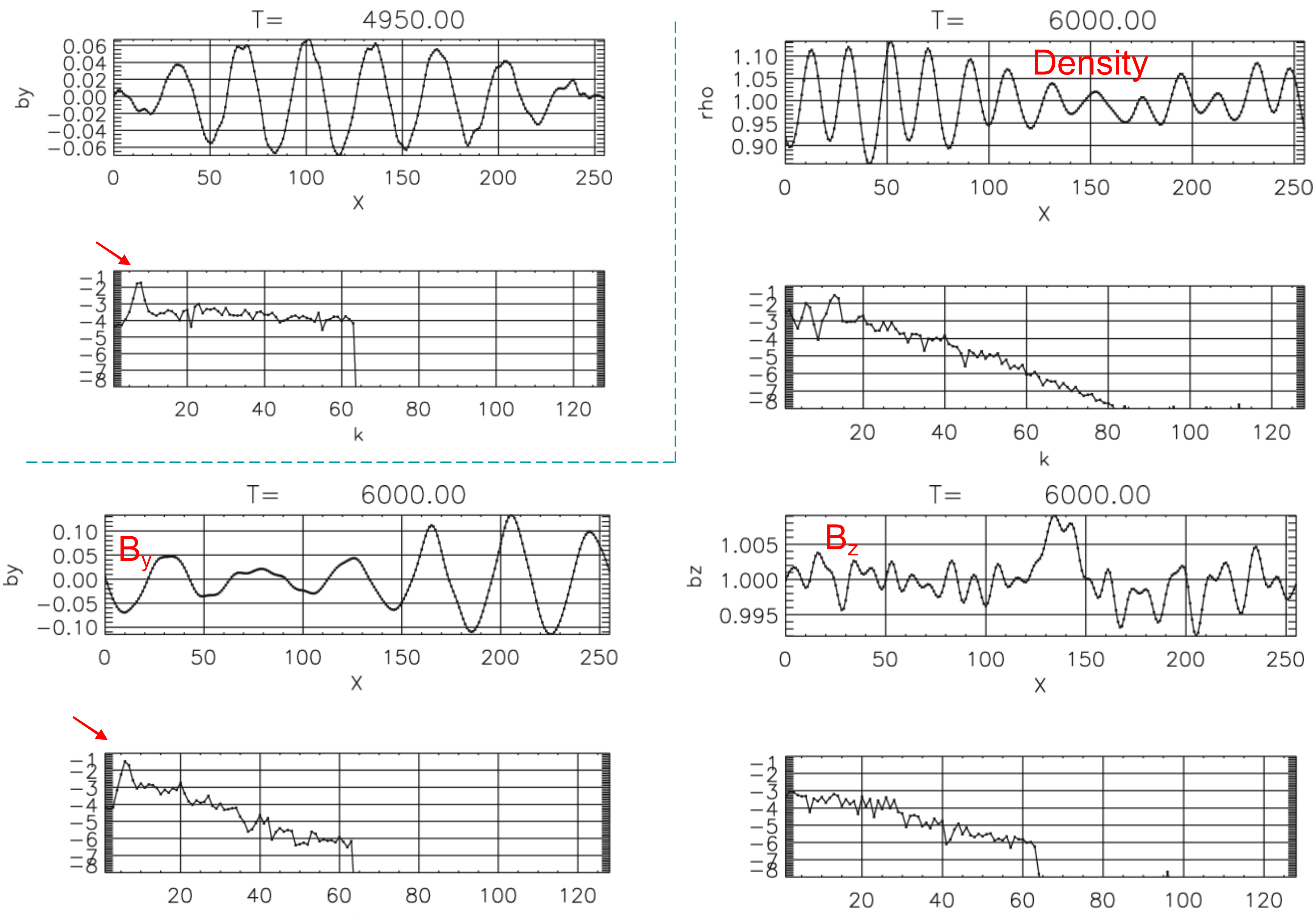

The b_z spectrum is flatter: turbulence of magnetosonic modes.

The density mode $2k_0$ is highly excited and often dominates.

Time evolution of the mean parallel electron temperature: heating by Landau damping

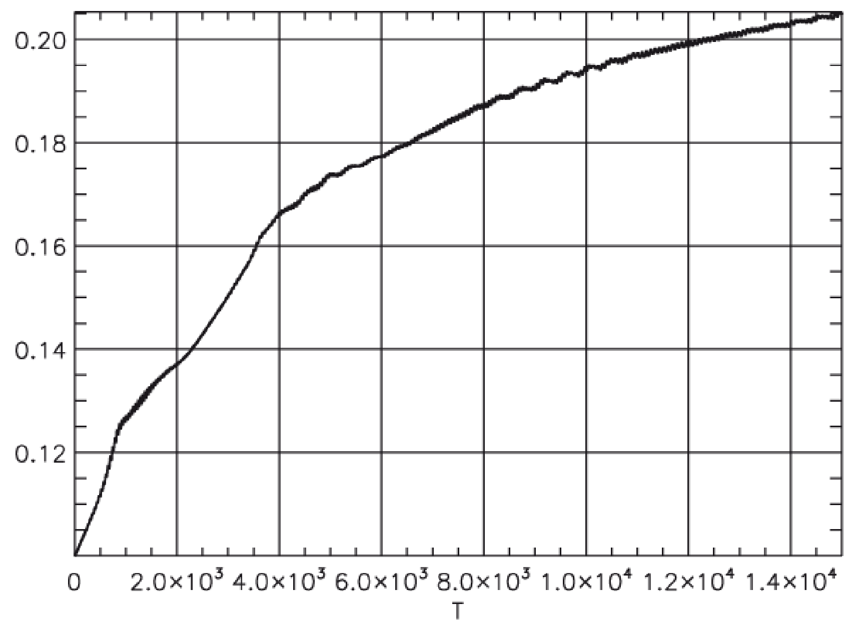

Time evolution of the mean parallel ion temperature: due to the inverse cascade

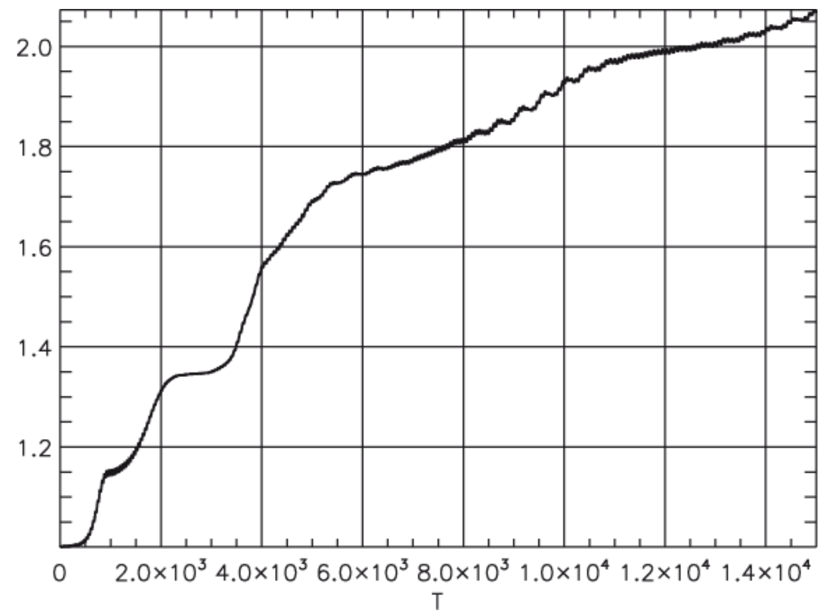

Perpendicular temperatures remain constant

III - *Intermediate case* where **low and high-k instabilities** coexist,

(β=0.01, b_0 =0.1, θ=87,1^o, $T_e/T_i=10^{-3}$ and $k_{\perp 0}\rho_i$ =0.2)

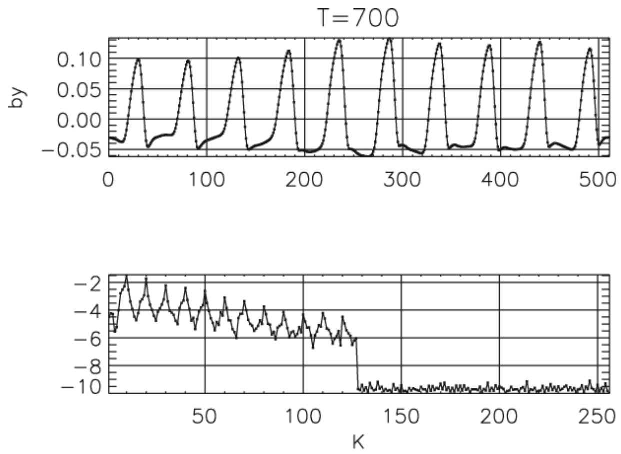

The b_y profile becomes very nonlinear while the wave starts propagating backward with modulation at a lower k-value

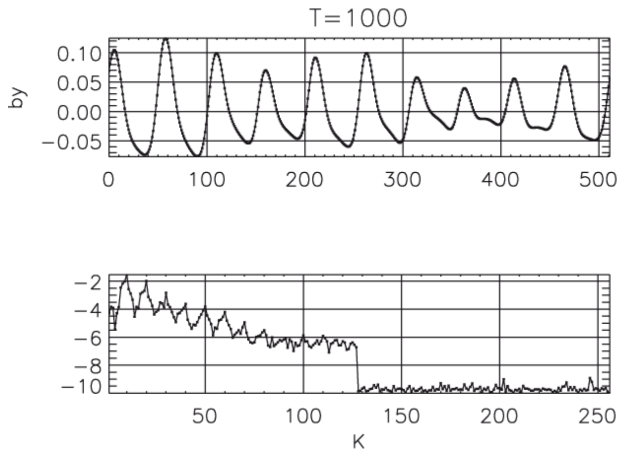

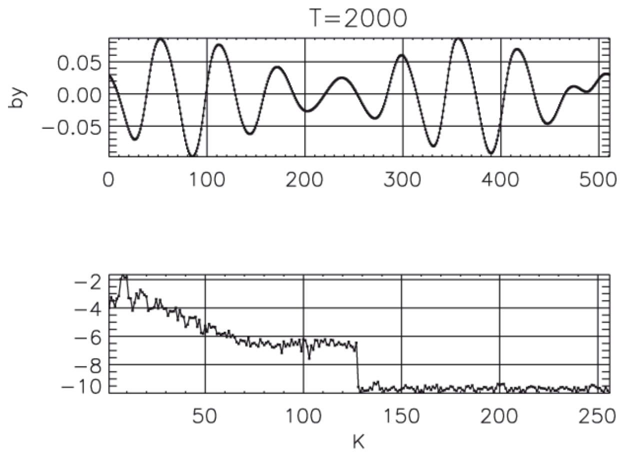

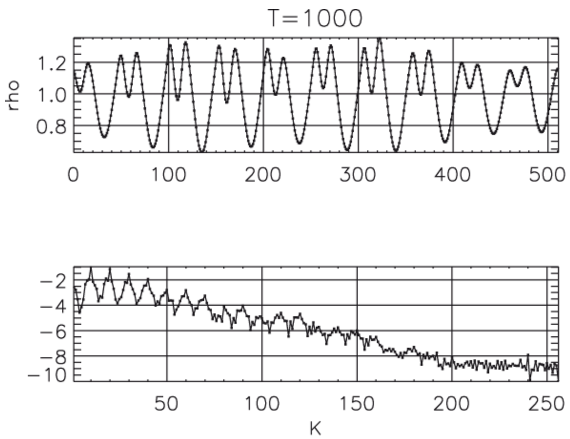

Large amplitude
density fluctuations

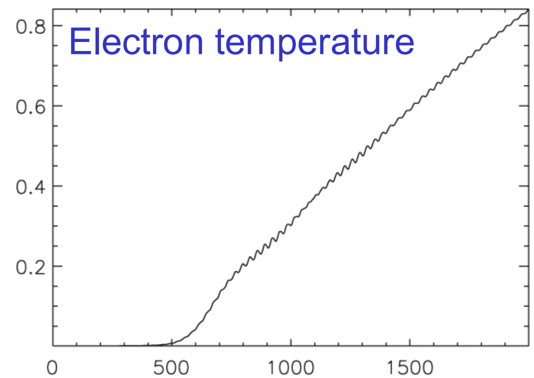

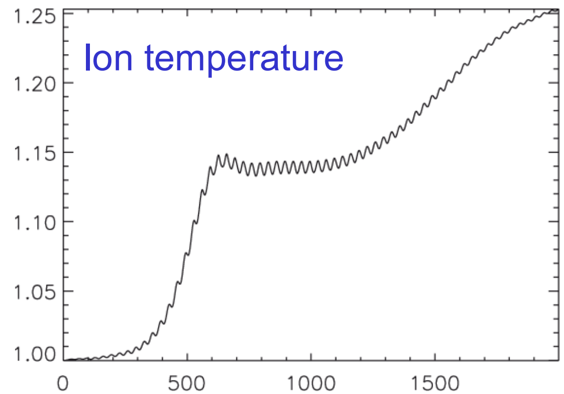

The previous results can be partly interpreted using the theory of Voitenko JPP 60, 497 (1998)
JPP 60, 515 (1998)

Calculations on the Vlasov equations at small β show that the decay process is of the form :

KAW -> KAW + KAW

Gowth rate varies like $k_\perp^2$ both in the $k_\perp \rho_i$ <<1 and $k_\perp$ ρi >>1 limits.

small wavelength domain: decay more effective into waves propagating in the same direction.

long wavelength domain: decay more effective into conter-propagating waves.

Amplitude threshold for decay decreases with higher k

=> KAW become nonlinear at very small amplitude.

Weak KAW turbulence induced by
3-wave interactions among waves propagating in the same direction, has
an inverse cascade for $k_\perp \rho_i$ <1 and a direct cascade for $k_\perp \rho_i$ >1
3-wave interactions among counter-propagating waves (usually more effective) results in an
inverse cascade over the whole $k_\perp$ range.

Quantitative discrepencies due to 1D: the most unstable modes lie at ~ 45^o from (k,B_0)-plane :
3D simulations are needed.

SUMMARY

FLR-Landau fluid model

- extends the Landau-fluid model developed by Snyder et al. (1997) for (non-dispersive) MHD scales, to quasi-transverse kinetic scales

- retains all the hydrodynamic nonlinearities, but kinetic effects (Landau damping and FLR corrections) are treated (quasi-)linearly

- provides an accurate description of the dispersion and collisionless damping of the low-frequency waves

- reproduces decay and modulational instabilities and their nonlinear developments

- can address a broad range of parameters and degrees of anisotropy

- should be useful for simulations of turbulence in a collisionless magnetized plasma for a range of scales extending from hydrodynamic scales to a fraction of the ion Larmor radius (work in progress).